Spectra of globular clusters in the Sombrero galaxy: evidence for spectroscopic metallicity bimodality[⋆]

Alan Alves-Brito[1,2]†, George K.T. Hau[1,3], Duncan A. Forbes[1], Lee R. Spitler[1]
Jay Strader[4], Jean P. Brodie[5], Katherine L. Rhode[6]

[1] *Centre for Astrophysics and Supercomputing, Swinburne University of Technology, Hawthorn, Victoria 3122, Australia*
[2] *PUC, Departamento de Astronomia y Astrofisica, Av. Vicuna Mackenna 4860, Santiago, Chile*
[3] *European Southern Observatory, Alonso de Cordova 3107, Vitacura, Santiago, Chile*
[4] *Harvard-Smithsonian Centre for Astrophysics, 60, Garden St., Cambridge, MA 02144, USA*
[5] *UCO/Lick Observatory, University of California, Santa Cruz, CA 95064, USA*
[6] *Department of Astronomy, Indiana University, Bloomington, IN 47405, USA*

ABSTRACT

We present a large sample of over 200 integrated-light spectra of confirmed globular clusters (GCs) associated with the Sombrero (M104) galaxy taken with the DEIMOS instrument on the Keck telescope. A significant fraction of the spectra have signal-to-noise levels high enough to allow measurements of GC metallicities using the method of Brodie & Huchra (1990). We find a distribution of spectroscopic metallicities ranging from $-2.2 < $ [Fe/H] $ < +0.1$ that is bimodal, with peaks at [Fe/H] ~ -1.4 and -0.6. Thus the GC system of the Sombrero galaxy, like a few other galaxies now studied in detail, reveals a bimodal *spectroscopic* metallicity distribution supporting the long-held belief that colour bimodality reflects two metallicity subpopulations. This further suggests that the transformation from optical colour to metallicity for old stellar populations, such as GCs, is not strongly non-linear. We also explore the radial and magnitude distribution with metallicity for GC subpopulations but small number statistics prevent any clear trends in these distributions.

Key words: globular clusters: general, galaxies: individual: Sombrero (M104: NGC 4594), galaxies: star clusters.

1 INTRODUCTION

Understanding how galaxies were formed and have evolved remains one of the basic problems to be solved in astrophysics. In this context, extragalactic globular clusters (GCs) play an important role because their formation is associated with the physical processes occurring before galaxies were entirely assembled (see Brodie & Strader 2006 for a review).

It has been recognised for some time that massive galaxies have bimodal GC colour distributions (Ashman & Zepf 1993). This suggests two modes, or phases, of GC formation. Indeed, several models have been proposed to explain the different modes in terms of variations in the epoch of GC formation, stellar population properties and the timescale of galaxy assembly (Ashman & Zepf 1992; Zepf & Ashman 1993; Forbes et al. 1997; Cote et al. 1998; Beasley et al. 2002). As most GCs appear to be very old (see review by Brodie & Strader 2006), the bimodality in colour is normally assumed to translate directly into a bimodality in metallicity. However, doubt has recently been cast on this interpretation by some (e.g. Yoon et al. (2006; Blakeslee, Cantiello & Peng 2010). Depending on the degree to which the transformation of colour into metallicity is non-linear, it is possible for an instrinsically unimodal metallicity distribution to appear bimodal in colour space. If correct, this would have direct implications for the observed blue tilt (a trend for redder colours with higher luminosities in the blue GC subpopulation) and the correlation of the mean GC colour with galaxy luminosity. It would also radically change current ideas for two modes of GC formation.

As noted by Blakeslee et al. (2010), *"Very little is actually known about the detailed metallicity distributions of GCs in giant ellipticals."*. Two giant ellipticals with optical spectroscopic metallicities derived for their GC systems include M49 with 47 measurements (Strader et al. 2007) and NGC 5128 with over 200 GC spectroscopic metallicities (Beasley et al. 2008). In both cases the distribution of GC spectroscopic metallicities are bimodal. The GC systems of these galaxies also have bimodal optical colour distributions, as do most but not all galaxies (see e.g. Foster et al. 2010). Interestingly, the infrared study of GCs in NGC 5128 by Spitler et al. (2008), which is more sensitive to metallicity than optical colours, also revealed colour bimodality in the 146 GCs they studied. Along similar lines, Kundu & Zepf (2007) used optical-infrared colours of 80 GCs in M87 to show their distribution was bimodal. Thus these giant ellipticals with optical spectra and/or infrared colours of GCs show metallicity bimodality.

Recently attempts have been made to derive spectroscopic metallicities using the infrared Calcium Triplet (CaT) lines (at 8498, 8542, and 8662 Å) for the GC systems of two giant ellipticals (Foster et al. 2010, 2011). In the case of NGC 1407, the CaT metallicity distribution of 144 GCs is better described as unimodal, whereas Cenarro et al. (2007) suggested that the distribution was bimodal based on metallicities from optical wavelength spectra of just 20 GCs. For NGC 4494, the CaT metallicity distribution again appears unimodal. Unfortunately, there is no published work based on optical wavelength metallicities for the GC system in this galaxy. Clearly a large sample study of GC metallicities derived from both blue and infrared absorption lines is needed to resolve these issues (see Foster et al. 2010 for a complete discussion of potential factors affecting the CaT derived metallicities). In summary, it appears that at least *some* elliptical galaxies reveal the presence of two metallicity subpopulations in their GC systems but the number of systems studied remains small.

For late-type spiral galaxies, only two are well-studied (i.e. the Milky Way and M31) and both reveal bimodal spectroscopic metallicity distributions for their GC systems (e.g. Zinn 1985; Barmby et al. 2000 but see also Caldwell et al. 2011). No early-type spirals have published spectra for large numbers of GCs.

The nearest spiral galaxy with a large GC system is the Sombrero galaxy (M104, NGC 4594), which lies a distance of 9.0 ± 0.1 Mpc (see Table 4 of Spitler et al. 2006 for a summary). Although classified as an edge-on Sa galaxy, it has a bulge-to-total ratio of 0.8 (Kent 1988) and hence might be better described as a massive bulge plus an extended disk. This galaxy hosts some 1900 GCs that extend to a projected radius of 50 kpc (Rhode & Zepf 2004; Spitler et al. 2006) and one Ultra Compact Dwarf (Hau et al. 2009). A number of previous studies have obtained spectra of Sombrero GCs (Bridges et al. 1997; Larsen et al. 2002; Held et al. 2003; Bridges et al. 2007), however the number of spectra of sufficient signal-to-noise (S/N) to measure individual GC metallicities was very limited. The Keck spectra of Larsen et al. (2002) confirmed that the dozen luminous GCs they studied were all old.

In this paper we present Keck integrated spectra for over 200 globular clusters in M104. This is the largest sample of GCs in the Sombrero galaxy homogeneously analysed to date. Our main goal is to obtain radial velocities to confirm association with the Sombrero galaxy and to obtain spectroscopic metallicities. A future paper will investigate the kinematic properties of the GC system.

2   OBSERVATIONS AND DATA REDUCTION

GC candidates were selected from two published photometric studies. In the inner regions we used the BVR HST/ACS mosaic of Spitler et al. (2006), which covers approximately the central $10' \times 7'$ of the galaxy with minimal contamination. Beyond this area, we used the ground-based BVR catalogue of Rhode & Zepf (2004). This latter catalogue has higher contamination but extends to the apparent edge of the GC system at a projected radius of $19'$ and so is necessary to complement the wide field-of-view ($16' \times 5'$) of the DEIMOS spectrograph. The central dust lane of NGC 4594 was excluded from our target selection.

Target selection was made using both magnitude and colour. The colour selection using the BVR filters was performed using previously published GCs as a guide (Bridges et al. 1997; Larsen et al. 2002; Held et al. 2003; Bridges et al. 2007). Four masks were designed, with a total of 404 GC candidates. The median candidate had $V \sim 22$ with both colour subpopulations well-represented. The masks included candidates with a wide radial range (extending to $\sim 11'$) and a moderate range in position angle, with the NE and SW quadrants of the galaxy well-covered.

All four masks were observed during a single run from 2006 April 26–29. Total exposure times for each mask ranged from 3–4.5 hr, divided into individual exposures of 30 min. All spectroscopic observations were made with the 900 l/mm grating, blazed at 5500 Å. Slits were milled to a width of $1.0''$, yielding a resolution of 2.1 Å (FWHM). Seeing was variable during the run, ranging from 0.6–$1.1''$.

The DEIMOS data were reduced using the DEEP2 `spec2d` package, adapted for our instrument setup. The nominal spectral coverage for an object in the center of the mask was ~ 3700–6900 Å, but the throughput toward the blue was low, so the useful spectral range was somewhat smaller. The wavelength scales were calibrated using arc spectra and fitting a 4th degree polynomial to the wavelength solution. The spectra were divided into two regions ("blue" and "red") and the wavelength solutions calculated separately, with an RMS scatter of 0.08 Å in the blue and 0.06 Å in the red, corresponding to roughly 5 and 3 kms^{-1} respectively. The presence of bright sky lines in the red spectra also allowed a correction for any instrument flexture between the science data taken during the night and the arcs taken during the day. Examples of the final spectra are given in Fig. 1.

3   RESULTS AND DISCUSSION

3.1   Radial Velocity Measurements

Heliocentric radial velocities were obtained using the IRAF[1] task `fxcor`. Fxcor performs Fourier cross-correlation of in-
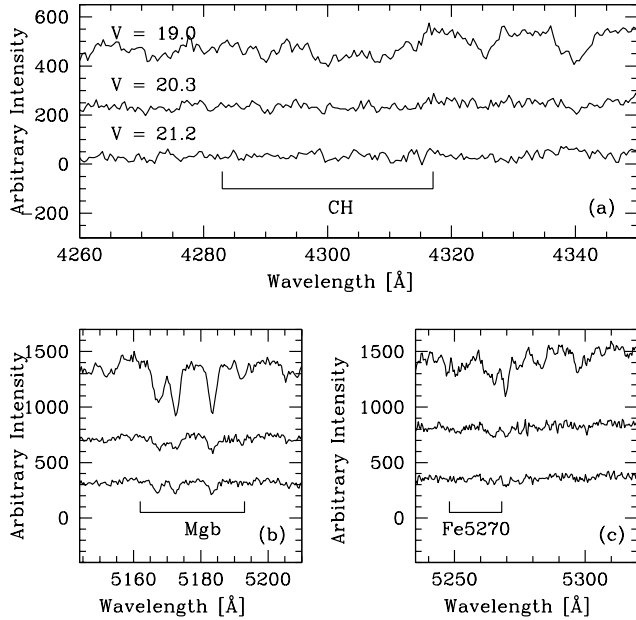

Figure 1. Example GC spectra obtained by the DEIMOS spectrograph. Shown are rest wavelength spectra around the metallicity sensitive indices of CH or G band (a), Mgb (b) and Fe5270 (c) for different GC magnitudes, as indicated in the figure.

Figure 2. Radial velocities of GC candidates. Velocity as a function of V band magnitude (a) and colour (b) are shown, along with the radial velocity distribution (c). The horizontal lines in (a) and (b) mark the mean v_r value (solid line) and the 1σ dispersion (dotted lines).

put object spectra against a specified template spectrum. For the cross-correlation of the DEIMOS spectra we used the spectrum of the K giant star Arcturus as the template.

We were able to measure radial velocities for 258 GC candidates. Data for all of the objects for which we could measure a radial velocity are presented in Table A. In this table, columns 1 and 2 indicate the object's ID (taken from either Spitler et al. 2006 or Rhode & Zepf 2004, indicated as S or RZ respectively); column 3 the mask number; columns 4–5 give the J2000.0 equatorial coordinates; columns 6–8 give the major- (X), minor-axis (Y) and the projected distances (R_p), respectively, from the centre of the galaxy; columns 9–10 give the radial velocities and their errors. The final velocity listed is the mean of the blue and red velocities, corrected to heliocentric. The uncertainties quoted are derived from the width of the cross-correlation peak, normalized using the distribution of the differences between the blue and red velocities as a function of magnitude, with a minimum value of 8 kms^{-1}. These uncertainties primarily reflect the random component of the error; we estimate our systematic error, due primarily to zero-point uncertainties, to be $\leqslant 20$ kms^{-1}.

To obtain the galactocentric coordinates (X,Y) and projected distances for our sample we adopted a distance to Sombrero of 9.0 Mpc (Spitler et al. 2006). At this distance, 1 arcmin corresponds to ~ 2.62 kpc. We used a central position of $\alpha_{J2000} = 12^h39^m99^s.43$, $\delta_{J2000} = -11°37'23"$. The position angle for the X-coordinate is taken as 90° (e.g., de Vaucouleurs et al. 1991). Hence, we are able to probe the Sombrero GC system out to ~ 30 kpc.

Figure 2 shows the radial velocities as a function of V magnitude, $B - R$ colour, and the radial velocity distribution for the 258 GC candidates. The mean velocity of the GC candidate sample is $v_r = 1075 \pm 359$ kms^{-1}. This is similar to the systemic velocity of Sombrero itself (1024 kms^{-1}; Smith et al. 2000). Furthermore, the radial velocity distribution for the bulk of the objects is roughly Gaussian, which is expected for a bound GC system. Thus we can conclude that the bulk of the objects with measured velocities are probable members of the Sombrero GC system. The tail of objects with very low and high radial velocities in this figure are likely foreground stars and background galaxies respectively. Given the clear gap between the bulk of the objects and those with high velocities, we have chosen to restrict our sample to $v_r < 2000$ kms^{-1} (the highest measured velocity, at ~ 3800 kms^{-1}, is likely spurious). We note that the GC candidates show no obvious trend of velocity with either magnitude or colour.

Figure 3 displays the radial velocities versus the projected galactocentric distance for GC candidates. The bulk of objects have velocities around 1100 kms^{-1} irrespective of galactocentric distance, although the dispersion decreases with radius. Such behaviour is similar to that seen by Bridges et al. (2007) in their study of the Sombrero GC system.

We exclude a further 14 objects with low velocities that lie at large projected distances (these are likely to be foreground stars). There are also five objects at large distances with somewhat higher velocities than the spread in velocities at that radius. These objects may be GCs with anomalous velocities. For the purposes of this spectroscopic metallicity analysis we adopt a conservative approach and exclude

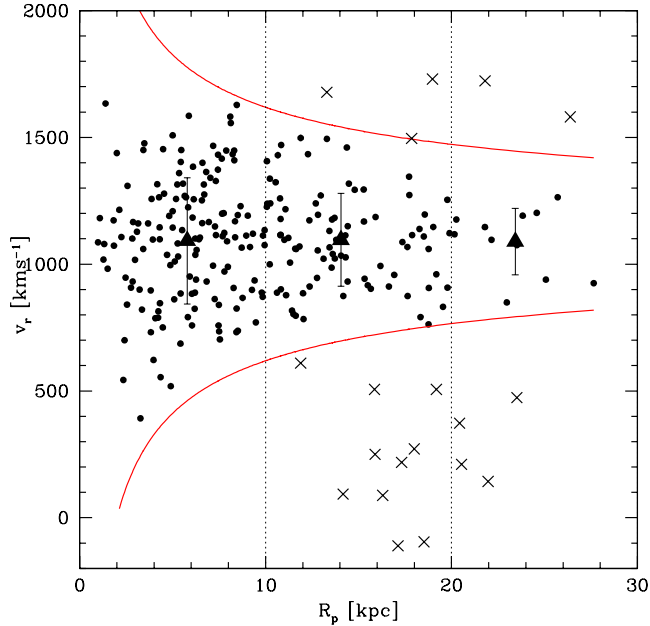**Figure 3.** Radial velocities for the Sombrero GC candidates against projected galactocentric distance. The final sample of confirmed GCs are shown by filled circles. Excluded objects are represented by crosses. The filled triangles indicate the median and dispersion of the radial velocities in different radial bins, as marked by the vertical dotted lines. The pair of solid lines shows a $R^{-1/2}$ dependence to guide the eye.

them from selection. For a kinematic analysis, in which outliers can have a large effect on results, a more sophisticated selection process will be required.

To quantify the velocity dispersion we binned our sample into three different radii ($0 < R_p \leqslant 10$ kpc, $10 < R_p \leqslant 20$ kpc and $R_p > 20$ kpc), which was a purely arbitrary choice. We measure $\sigma_r = 249$ kms^{-1} in the first bin, $\sigma_r = 183$ kms^{-1} in the second, and $\sigma_r = 131$ kms^{-1} in the third one. The excluded objects lie at least 2σ away from the mean velocity in each bin.

After excluding the probable foreground stars, background galaxies and high velocity objects we have a sample of 239 velocity confirmed GCs associated with the Sombrero galaxy.

We have reliable radial velocities for 37 GCs with previously published data. We compare our new velocities to those from the literature in Fig. 4, in which the different studies are coded by symbol type. Nearly all of the repeats are from the 2dF and WHT studies of Bridges et al. (1997; 2007). There is no evidence for a zeropoint offset in the velocity scales, with median differences (in the stated sense of new−old) of −3 and −17 kms^{-1} for the two studies respectively. In addition, the distribution of velocities differences generally seems consistent with that expected from the stated uncertainties, excepting a small number of outliers. The radial velocities from Larsen et al. (2002) are systematically higher than ours (−78 in the median), but with only four GCs in common, this conclusion is not strong.
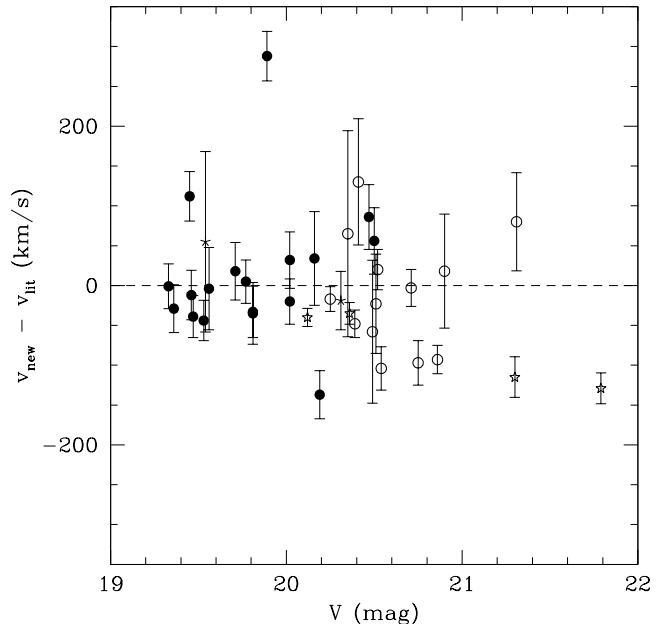
Figure 4. Radial velocity difference between our new measurements and values in the literature for the 37 GCs in common. The symbols represent the different literature datasets: filled circles (2dF, Bridges et al. 2007); open circles (WHT, Bridges et al. 1997); open stars (Keck, Larsen et al. 2002); skeletal stars (WIYN, Bridges et al. 2007).

3.2 Metallicity Analysis

In order to derive spectroscopic metallicities for our moderate resolution and moderate signal-to-noise (see Fig. 1) data we adopt a similar approach to that of Perrett et al. (2002) and Brodie & Huchra (1990) who studied the GCs of M31. Aiming to measure the metallicities of extragalactic GCs, Brodie & Huchra (1990, hereafter BH90) defined a set of calibrations based upon six different absorption-line indices, which were strongly sensitive to metallicity. Their metallicity calibrations were tied to the Milky Way GC system and therefore the assumption that the GCs are mostly old (i.e. $\geqslant 10$ Gyr).

Originally, BH90 measured the metallicity of globular clusters by taking the weighted mean of the six elemental absorption-line indices, which lead to estimated metallicities with an accuracy of approximately 15 per cent. However, Perrett et al. (2002) used the same method employed by BH90 but extended their analysis to 12 absorption-line indices. Comparing the line indices with published (and independent) metallicities of GCs in M31, Perrett et al. (2002) found that the CH (G Band), Mgb and Fe53 line indices were the best metallicity calibrators. Consequently, they calculated the final metallicities of their sample by adopting an unweighted mean of these best [Fe/H]-indicators.

As we are dealing with uncalibrated flux spectra, we have preferentially used the relatively narrow metallicity indices CH, Mgb and Fe5270, as they are less sensitive to index calibration errors. In addition, CH and Mgb constitute some of the strongest features in the integrated spectra of late-type objects. However, it is worth emphasizing that due to the different slit positions in the masks, the DEIMOS spec-
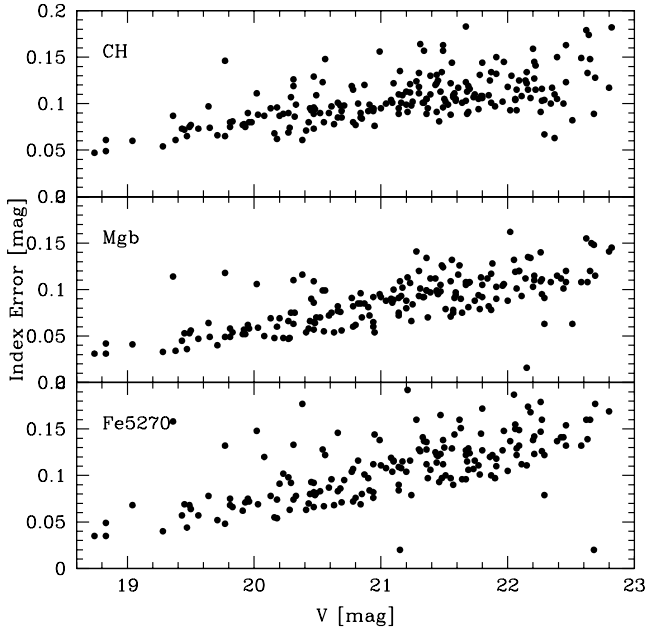
Figure 5. Index error versus GC magnitude. Three indices are shown with CH (*top*), Mgb (*middle*) and Fe5270 (*bottom*).

Figure 6. Colour-metallicity relations based on B-R colours and CH (*top*), Mgb (*middle*) and Fe5270 (*bottom*) indices.

tra cover different wavelengths, and thus it was not possible to calculate the three indices for all GCs.

The feature passbands, pseudocontinua and [Fe/H]-calibrations adopted in this work are exactly as defined in BH90. The three indices were measured automatically by employing a modified version of the LECTOR code, which was made available by Alexandre Vazdekis. The code takes into account the index-band definitions (see Table 1) and the radial velocities to calculate the line indices and their errors accordingly. In Fig. 1 we show the location of the three indices on example spectra.

In Table B we list the GC magnitudes, colours, raw indices and spectroscopic metallicities obtained by following the prescription above. The values given in brackets (when possible) correspond to the estimated uncertainty on the indices and metallicities. The former corresponds to the Poisson noise errors, while the latter was estimated by propagating these errors and those associated with the metallicity calibrations themselves (see last column of Table 1) in quadrature. Note, however, that these uncertainties could be underestimated since we are not taking into account other possible sources of error. In Fig. 5 we show the Poisson errors as a function of magnitude for each index. As expected, the uncertainties are higher for the fainter objects, since they have lower S/N.

In Fig. 6 we plot the derived [Fe/H] metallicity from each individual index against the B–R colour. In old stellar populations, colour is a good proxy for metallicity. This figure shows that all three indices reveal similar trends with respect to B–R colour. The scatter for the Mg and Fe5270 indices are similar. The scatter for the CH index is somewhat larger this is because it is a wider index and located at bluer wavelengths for which DEIMOS is less sensitive. We combine the individual [Fe/H] values, weighted by their errors, to form a final metallicity of each GC.
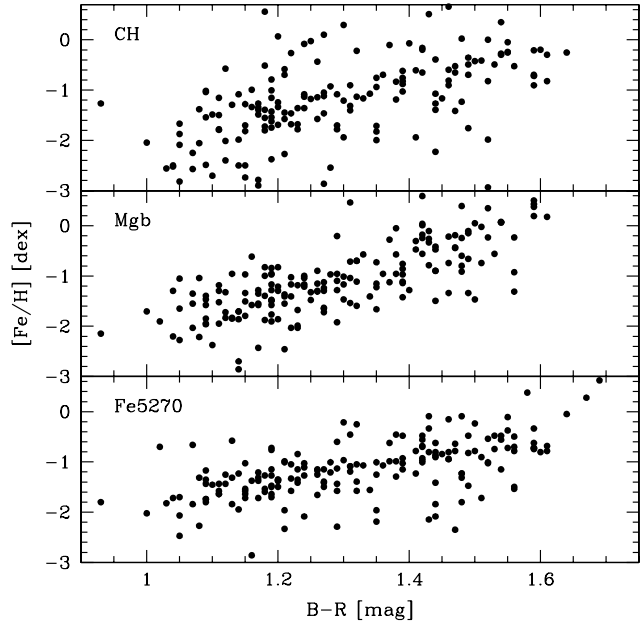
For the subsequent metallicity analysis, we have restricted our sample to the brightest objects (i.e. V ⩽ 22 mag) and those with Poisson errors < 0.15 dex (see Fig. 5). After excluding these lower S/N GCs, the remaining 112 GCs have a metallicity range of −2.2< [Fe/H] < +0.1. Interestingly, Spitler et al. (2006) found the $B - R$ and $B - V$ colours to give similar metallicity ranges of –2.1 < [Fe/H]$_{B-R}$ < 0.3 and –2.3 < [Fe/H]$_{B-V}$ < +0.4, respectively, based on data from the HST/ACS. Hence, within the uncertainties, the spectroscopic metallicities we derive here are in good agreement with the photometric ones. For example, the mean spectroscopic metallicity of [Fe/H] $\sim$ –1.2 agrees well with that estimated previously by Bridges et al. (1997, 2007) and Larsen et al. (2002). Furthermore, the mean difference in [Fe/H] for the four globular clusters in common with those studied in Larsen et al. (2002) is only –0.14 ± 0.07 dex (our - theirs), which is small within the uncertainties.

3.3 Metallicity Distribution

In order to test for the presence of bimodality in the GC metallicity distribution we have employed the KMM algorithm. The KMM algorithm (see Ashman, Bird & Zepf 1994 for details) returns the likelihood ratio test statistic and calculates the probability P of a distribution being unimodal (single Gaussian) or bimodal (double Gaussian model). It is independent of data binning.

For a homoscedastic fit to the $B - R$ colours we find that the colour distribution for our sample of 239 spectroscopically-confirmed GCs in the Sombrero galaxy is bimodal at a confidence level of greater than 99.7 per cent (see Fig. 7). The blue and red peaks are at $B - R = 1.19$ and 1.46 mag, respectively. Thus we are sampling a bimodal colour distribution of GCs.

In Fig. 8 we show the relationship between GC colour

Table 1. Definition of BH90 indices and metallicity calibrations.

Index	Blue [Å]	Feature [Å]	Red [Å]	Width [Å]	[Fe/H] calibration
CH	4268.25-4283.25	4283.25-4317.00	4320.75-4335.75	33.25	[Fe/H] = 11.415×(CH) −2.455 (σ = 0.26)
Mgb	5144.50-5162.00	5162.00-5193.25	5193.25-5207.00	31.25	[Fe/H] = 14.171×(Mgb) −2.216 (σ = 0.35)
Fe5270	5235.50-5249.00	5248.00-5268.75	5288.00-5319.25	20.75	[Fe/H] = 20.367×(Fe5270) −2.086 (σ = 0.33)
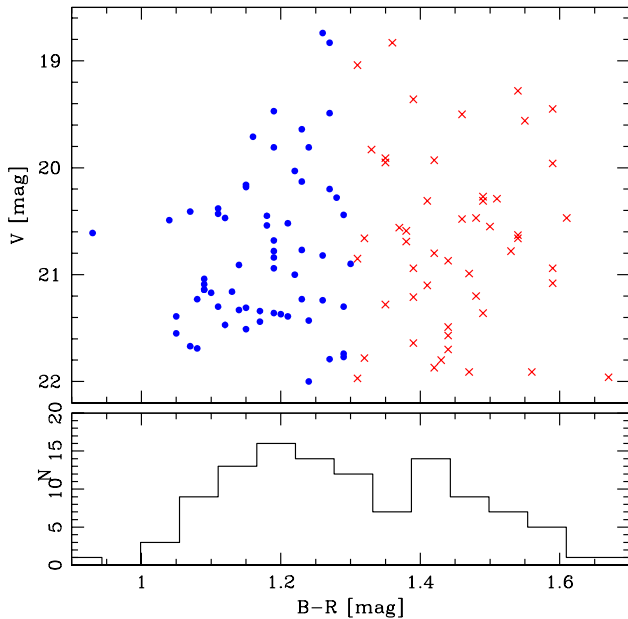
Figure 7. Colour-magnitude diagram (*top*) and the colour histogram (*bottom*) for 112 GCs. The blue points and red crosses represent blue and red GC subpopulations cut at B–R = 1.30 respectively.

Figure 8. Colour-metallicity relation (*top*) and metallicity histogram (*bottom*) based on spectroscopic metallicities. The least-squares linear fit is shown by a black solid line. The red dotted line indicates the linear colour-metallicity relation found by Barmby et al. (2000) for the GC system of M31. The colour-metallicity relations predicted by SSP models are also shown, i.e. Teramo-SPoT (Raimondo et al. 2005; blue short dashed line) and Maraston (1998; green long dashed line).

and our derived mean spectroscopic metallicity. The figure shows a good correlation between colour and metallicity with no obvious indication that the relationship is non-linear. A least-square linear fit to the data gives [Fe/H] = (−4.83 ± 0.27) + (2.85 ± 0.20)×(B-R) with σ = 0.33 dex, for 1 ⩽ (B-R) ⩽ 1.65. The rms dispersion in the relation is comparable to that for the conversion of the raw BH90 indices into metallicity. We also show the linear relation of Barmby et al. (2000) who used the BH90 indices for GCs in M31. For comparison, we have also overplotted the colour-metallicity relations predicted by the old age simple stellar population (SSP) models of the Teramo-SPoT group (Raimondo et al. 2005) and Maraston (1998). All provide a reasonable description of the data, albeit with small offsets from the least-square best fit.

For a KMM fit to the spectroscopic metallicities, we find bimodality with a probability > 90 per cent, where the metal-poor subpopulation is peaked at [Fe/H] = −1.44 and the metal-rich one at [Fe/H] = −0.60. These values can be compared to [Fe/H] = −1.38 and -0.49 quoted by Spitler et al. (2006) based on optical colours and [Fe/H] ∼ −1.7 and −0.7 from Held et al. (2003) from spectra.

3.4 Radial Metallicity Profile

Currently very few galaxies have published radial metallicity profiles for GCs based on spectroscopy. In both the Milky Way (Harris 2001) and M31 (Alves-Brito et al. 2009), the GCs follow a similar pattern, i.e. a strong metallicity gradient in the inner few kpc, which then flattens to a null gradient in the outer halo. Similar metallicity profiles are inferred for GCs in large elliptical galaxies from their colours (see Forbes et al. 2011 and references therein). These metallicity profiles suggest an inner region in which gas dissipation has played an important role, and an outer halo region that is dominated by the accretion of small galaxies and their GCs.

In Fig. 9 we show the radial metallicity profile for the GCs in the Sombrero galaxy out to 30 kpc. There is no clear indication of metallicity gradients in either GC subpopulation. However, our data are not uniformly distributed in radius and are quite limited beyond 20 kpc. We note that the transition from a strong inner gradient to a null gradient in the massive ellipticals M87 (Harris 2009) and NGC
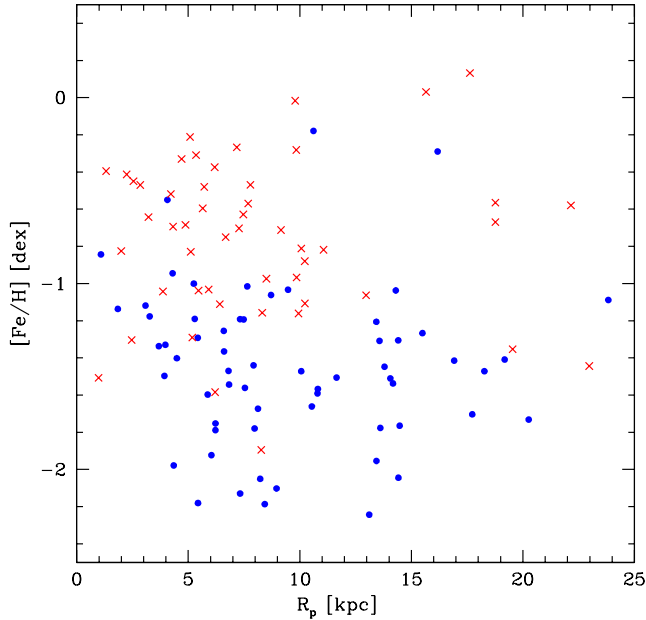
Figure 9. Metallicity as a function of projected galactocentric distance. Symbols are as in Fig. 6.

Figure 10. Metallicity-magnitude diagram. Symbols are as in Fig. 7.

1407 (Forbes et al. 2011) were seen at around 70 kpc. Given that the luminosity of Sombrero is more comparable to these galaxies than the Milky Way or M31, we might expect the transition radius to occur beyond our field-of-view.

3.5   Blue Tilt

It has been shown in several extragalactic GC systems that the blue GC subpopulation colour distribution tends to become redder for higher luminosities (i.e., a blue tilt). While this effect has been found in galaxies of different morphological types (e.g. Harris et al. 2006; Strader et al. 2006; Mieske et al. 2006; Lee et al. 2008; Harris 2009; Peng et al. 2009; Mieske et al. 2010; Forbes et al. 2010; Faifer et al. 2011), the Milky Way is a galaxy that do not reveal a blue tilt to date (e.g., Strader & Smith 2008). According to the scenario proposed by Bailin & Harris (2009), the more massive GCs are also more heavy-element enriched. Thus, the fact that the Milky Way sample includes fewer massive GCs and more lower mass GCs than other datasets, could account for the lack of tilt in the Milky Way.

On the other hand, Forbes et al. (2010) have recently shown that there is a blue tilt in the blue GC subpopulation of the Milky Way analog NGC 5170. For the Sombrero galaxy, Spitler et al. (2006) have shown photometrically that its blue GCs reveal a blue tilt not only at the brightest magnitudes (highest mass) but that it may also extend to relatively low mass GCs too. The blue tilt is generally assumed to be a mass-metallicity trend that is due to a self-enrichment process (Strader & Smith 2008; Bailin & Harris 2009).

We present in Fig. 10 the spectroscopic metallicity-magnitude diagram for Sombrero GCs. It shows that the brightest GCs have magnitudes comparable to Omega Cen which would have V ∼ 19.5 if located at the distance of Som-

brero. Although the brightest blue GCs are more metal-rich than average, our number statistics are too low to make any definitive statements about a spectroscopic 'blue tilt' in the Sombrero galaxy GC system. In the self-enrichment models mentioned above the tilt is present for GCs with masses above a million solar masses or V ⩽ 19.5.
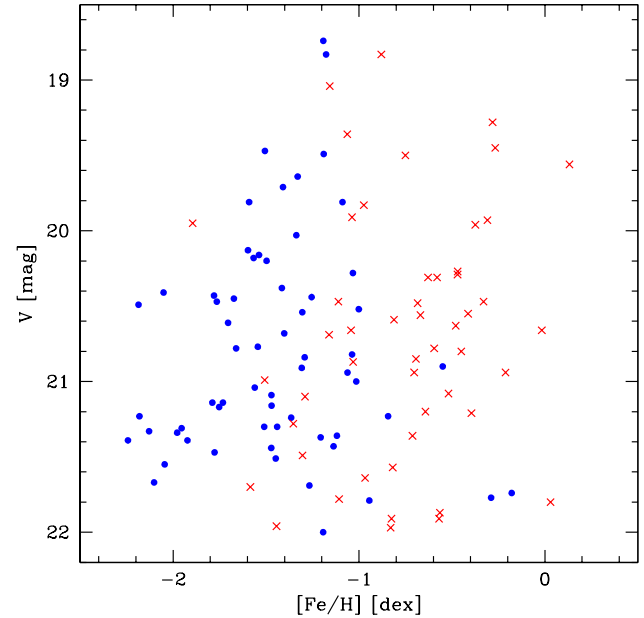
4   SUMMARY AND CONCLUSIONS

Globular clusters are widely recognised as extremely useful tracers of the formation and evolution of their host galaxies. Here we present Keck spectra for over 200 GCs with radial velocities that confirm their association with the Sombrero galaxy. For many of the GCs the spectra are of sufficient quality to derive Brodie & Huchra (1990) style metallicities from several indices.

We find that the GCs span a broad metallicity range from [Fe/H] = −2.2 to +0.1. This is comparable to previous estimates based on photometric metallicities. For a restricted high quality subsample of 112 GCs, we find a good correlation between individual GC metallicity and B–R colour. The resulting spectroscopic metallicity distribution is clearly bimodal with peaks at [Fe/H] ∼ −1.4 and −0.6, with a statistical probability of > 90 per cent. Thus despite claims that colour bimodality may not reflect metallicity bimodality in extragalactic GC systems, it would appear that the GC system of the Sombrero galaxy joins that of some other giant elliptical galaxies in revealing spectroscopic bimodality. Furthermore we find a transformation between optical colour and metallicity that does not require a non-linear relation.

We also investigate the GC radial metallicity profile out to 30 kpc and a spectroscopic version of the colour-magnitude diagram, but our small number statistics prevent

any strong statements about trends in the GC subpopulations.

REFERENCES

Alves-Brito A., Forbes D. A., Mendel J. T., Hau G. K. T., Murphy M. T., 2009, MNRAS, 395, 34

Ashman K. M., Zepf, S. E., 1992, ApJ, 384, 50

Ashman K. M., Zepf S. E., 1993, MNRAS, 264, 611

Ashman K. M., Bird C. M., Zepf S. E. 1994, AJ, 108, 2348

Bailin J., Harris W.E. 2009, ApJ, 695, 1082

Barmby, P., Huchra, J. P., Brodie, J. P., Forbes, D. A., Schroder, L. L., & Grillmair, C. J. 2000, AJ, 119, 727

Blakeslee J.P., Cantiello. M., Peng E.W. 2010, ApJ, 710, 51

Beasley, M. A., Baugh, C. M., Forbes, D. A., Sharples, R. M., & Frenk, C. S. 2002, MNRAS, 333, 383

Beasley M. A., Bridges T., Peng, E., Harris W.E., Harris G.L., Forbes D.A., Mackie G., 2008, MNRAS, 386, 1443

Bridges T. J., Ashman K. M., Zepf S. E., Carter D., Hanes D. A., Sharples R. M., Kavelaars J. J., 1997, MNRAS, 284, 376

Bridges T. J., Rhode K. L., Zepf S. E., Freeman K. C., 2007, ApJ, 658, 980

Brodie J. P., Strader J., 2006, ARA&A, 44, 193

Brodie J. P., Huchra J. P., 1990, ApJ, 362, 503

Caldwell, N., Schiavon, R., Morrison, H., Rose, J. A., & Harding, P. 2011, AJ, 141, 61

Cenarro, A. J., Beasley, M. A., Strader, J., Brodie, J. P., & Forbes, D. A. 2007, AJ, 134, 391

Cote, P., Marzke, R. O., & West, M. J. 1998, ApJ, 501, 554

Faifer, F. R., Forte, J. C., Norris, M.A., Bridges, T., Forbes, D. A., Zepf, S. E., Beasley, M., Gebhardt, K., Hanes, D. A., Sharples, R. M. 2011, arXiv1105.1755F

Forbes, D. A., Brodie, J. P., & Grillmair, C. J. 1997, AJ, 113, 1652

Forbes D.A., Spitler L.R., Harris W. E., Bailin J., Strader J., Brodie J. P., Larsen S. S. 2010, MNRAS, 403, 429

Forbes, D. A., Spitler, L. R., Strader, J., Romanowsky, A. J., Brodie, J. P., & Foster, C. 2011, MNRAS, 306

Foster, C., Forbes, D. A., Proctor, R. N., Strader, J., Brodie, J. P., & Spitler, L. R. 2010, AJ, 139, 1566

Foster, C. et al. 2011, MNRAS, submitted

Harris, W.E., in: Star Clusters, Saas-Fee Advanced Course 28. Edited by L Labhardt and B. Binggeli. Published by Springer-Verlag, Berlin, 2001, p.223

Harris W.E., Whitmore B.C., Karakla D., Okón W.; Baum W. A., Hanes D.A., Kavelaars J.J. 2006, ApJ, 636, 90

Harris W.E. 2009, ApJ, 703, 939

Hau, G.K.T., et al. 2009, MNRAS, 394, L97

Held E.V., Moretti A., Federici L., Cacciari C., Rizzi L., Testa V. 2003, in: Extragalactic Globular Cluster Systems: Proceedings of the ESO Workshop, Edited by M. Kissler-Patig. Springer-Verlag, p. 161

Kent S., 1988, AJ, 96, 514

Kundu A., Zepf, S., 2007, ApJ, 660, L109

Larsen S.S., Brodie J.P., Beasley M.A., Forbes D.A., 2002, AJ, 124, 828

Lee M.G., Park H.S., Kim E., Hwang H.S., Kim S.C., Geisler D. 2008, ApJ, 682, 135

Maraston, C. 1998, MNRAS, 300, 872

Mieske S., Jordán A.; Côté P., Kissler-Patig M., Peng E. W., Ferrarese L., Blakeslee J. P., Mei S., Merritt D., Tonry J. L., West M.J. 2006, ApJ, 653, 193

Mieske, S., Jordán, A., Côté, P., Peng, E. W., Ferrarese, L., Blakeslee, J. P., Mei, S., Baumgardt, H., Tonry, J. L., Infante, L., West, M. J. 2010, ApJ, 710, 1672

Peng E. W., Jordán A., Blakeslee J.P., Mieske S., Côté P., Ferrarese L., Harris W. E., Madrid J.P., Meurer G. R. 2009, ApJ, 703, 42

Perrett K.M., Bridges, T.J., Hanes D.A., Irwin M.J., Brodie J.P., Carter D., Huchra J.P., Watson F.G., 2002, AJ, 123, 2490

Raimondo G., Brocato E., Cantiello M., Capacciolo M., 2005, AJ, 130, 2625

Rhode K., Zepf S.E. 2004, AJ, 127, 302

Smith, R. J., Lucey, J. R., Hudson, M. J., Schlegel, D. J., Davies, R. L. 2000, MNRAS, 313, 469

Spitler L. R., Larsen S., Strade J., Brodie J. P., Forbes D., Beasley M., 2006, AJ, 132, 1593

Strader J., Brodie J. P., Cenarro A.J., Beasley M., Forbes D. 2005, AJ, 130, 131

Strader J., Brodie J. P., Spitler L. R., Beasley M., 2006, AJ, 132, 2333 AJ, 132, 1593

Strader J., Beasley M.A., Brodie J.P. 2007, AJ, 133, 2015

Spitler, L. R., Forbes, D. A., & Beasley, M. A. 2008, MNRAS, 389, 1150

Strader J., Smith G.H. 2008, AJ, 136, 1828

Vazdekis A. 1999, ApJ, 513, 224

Yoon, S.-J., Yi, S. K., & Lee, Y.-W. 2006, Science, 311, 1129

Zepf, S. E., Ashman, K. M. 1993, MNRAS, 264, 611

Zinn, R. 1985, ApJ, 293, 424

APPENDIX A: POSITIONS AND VELOCITIES

APPENDIX B: MAGNITUDES, COLOURS, INDICES AND METALLICITIES

In Table B1 we present magnitudes, colours, indices and metallicities for the globular cluster candidates. The table is ordered by ID.

Table A1. IDs, positions and velocities for the sample.

ID	Alt ID	Mask	R.A. (J2000)	Dec. (J2000)	X (arcmin)	Y (arcmin)	R_p (arcmin)	V_r kms^{-1}	σV_r kms^{-1}
(1)	(2)	(3)	(4)	(5)	(6)	(7)	(8)	(9)	(10)
RZ1157	–	1	12 40 36.93	-11 41 17.55	9.224	-3.907	10.020	1581	49
RZ1191	–	1	12 40 36.35	-11 40 58.07	9.082	-3.582	9.763	1264	8
RZ1192	–	1	12 40 36.34	-11 39 33.72	9.079	-2.177	9.336	1202	10
RZ1210	–	1	12 40 36.03	-11 38 19.15	9.001	-0.933	9.049	1191	117
RZ1255	–	1	12 40 34.76	-11 38 10.23	8.689	-0.785	8.724	849	8
RZ1290	–	1	12 40 33.82	-11 36 19.31	8.689	−0.785	8.724	3844	57
RZ1308	–	1	12 40 33.20	-11 40 39.82	8.306	-3.278	8.930	1146	26
RZ1312	–	1	12 40 33.05	-11 37 00.33	8.269	0.379	8.277	1118	96
RZ1405	–	1	12 40 30.34	-11 36 27.93	7.601	0.919	7.657	1147	46
RZ1470	–	1	12 40 28.75	-11 36 58.42	7.211	0.411	7.222	1147	46
RZ1506	–	1	12 40 27.73	-11 36 22.31	6.959	1.013	7.032	−95	8
RZ1532	–	2	12 40 27.22	-11 39 54.60	6.835	-2.525	7.287	448	8
RZ1533	–	2	12 40 27.21	-11 40 30.03	6.833	-3.116	7.510	1254	9
RZ1567	–	1	12 40 26.38	-11 39 26.44	6.629	-2.056	6.940	1068	8
RZ1591	–	2	12 40 25.84	-11 40 18.94	6.496	-2.931	7.127	1060	12
RZ1632	–	2	12 40 24.88	-11 39 08.52	6.259	-1.758	6.501	-111	10
RZ1638	–	1	12 40 24.74	-11 39 50.67	6.225	−2.460	6.694	1068	8
RZ1661	–	1	12 40 23.88	-11 37 42.03	6.014	-0.316	6.022	506	17
RZ1690	–	1	12 40 23.30	-11 36 26.20	5.870	0.947	5.946	942	8
RZ1724	–	2	12 40 22.64	-11 41 03.78	5.709	-3.679	6.791	1115	20
RZ1733	–	1	12 40 22.31	-11 38 51.87	5.627	-1.480	5.819	1027	14
RZ1780	–	1	12 40 21.02	-11 38 38.41	5.311	-1.256	5.457	1460	11
RZ1836	–	1	12 40 19.90	-11 37 45.86	5.034	-0.380	5.049	1494	8
RZ1841	–	1	12 40 19.62	-11 38 58.04	4.966	-1.583	5.212	1022	32
RZ1923	S366	1	12 40 17.92	-11 38 32.06	4.549	-1.150	4.692	1173	8
RZ1934	–	2	12 40 17.73	-11 40 44.60	4.502	-3.360	5.617	1293	9
RZ1946	S214	1	12 40 17.36	-11 37 19.20	4.412	0.063	4.412	797	13
RZ1983	S228	3	12 40 16.63	-11 39 44.93	4.231	-2.365	4.847	946	19
RZ1990	S230	1	12 40 16.49	-11 38 18.33	4.198	-0.921	4.298	1006	9
RZ1997	S204	3	12 40 16.23	-11 39 11.67	4.135	-1.811	4.514	1498	26
RZ1998	–	2	12 40 16.19	-11 42 30.46	4.124	-5.124	6.577	218	13
RZ2014	S271	3	12 40 15.78	-11 37 39.30	4.022	-0.271	4.031	888	16
RZ2021	S047	1	12 40 15.58	-11 36 20.94	3.972	1.035	4.105	1116	8
RZ2024	–	2	12 40 15.53	-11 41 01.50	3.960	-3.641	5.380	93	9
RZ2037	S236	1	12 40 15.33	-11 38 40.17	3.910	-1.286	4.116	1470	8
RZ2038	S009	2	12 40 15.31	-11 40 12.70	3.907	-2.828	4.823	1240	8
RZ2055	–	2	12 40 15.04	-11 40 44.31	3.841	-3.355	5.100	1131	13
RZ2059	S211	2	12 40 14.99	-11 39 07.04	3.829	-1.734	4.203	1217	8
RZ2082	–	2	12 40 14.65	-11 41 55.43	3.745	-4.540	5.885	917	20
RZ2084	S197	1	12 40 14.63	-11 36 35.32	3.739	0.795	3.823	1226	11
RZ2106	S195	3	12 40 14.18	-11 38 25.64	3.630	-1.044	3.777	1075	15
RZ2109	S077	1	12 40 14.11	-11 38 38.38	3.611	-1.256	3.824	1406	8
RZ2144	S021	2	12 40 13.56	-11 39 34.44	3.477	-2.190	4.110	901	8
RZ2194	–	2	12 40 12.66	-11 41 29.43	3.254	-4.107	5.240	1096	16
RZ2237	–	4	12 40 11.74	-11 41 56.47	3.029	-4.558	5.473	931	13
RZ2242	S063	2	12 40 11.64	-11 38 14.44	3.003	-0.857	3.123	1434	8
RZ2276	S234	1	12 40 11.15	-11 37 45.37	2.884	-0.372	2.908	1199	10
RZ2289	S069	3	12 40 10.98	-11 35 54.64	2.842	1.473	3.201	732	13
RZ2303	S033	3	12 40 10.76	-11 40 00.64	2.789	-2.627	3.832	1239	10
RZ2305	S248	2	12 40 10.71	-11 39 08.62	2.775	-1.760	3.286	1229	10
RZ2307	S055	3	12 40 10.67	-11 36 45.30	2.766	0.628	2.836	759	11
RZ2316	–	4	12 40 10.52	-11 45 20.41	2.729	-7.957	8.412	1096	11
RZ2342	–	4	12 40 10.07	-11 42 11.61	2.618	-4.810	5.476	1150	20
RZ2344	–	4	12 40 10.05	-11 44 19.78	2.613	-6.946	7.421	832	21
RZ2363	S016	1	12 40 09.72	-11 36 22.55	2.533	1.008	2.726	1467	8
RZ2381	S019	1	12 40 09.35	-11 35 16.10	2.440	2.115	3.229	1195	8
RZ2390	S492	3	12 40 09.19	-11 35 54.00	2.402	1.483	2.824	1373	38
RZ2410	S093	1	12 40 08.83	-11 34 07.00	2.313	3.267	4.003	1323	11
RZ2428	–	4	12 40 08.53	-11 43 24.36	2.239	-6.022	6.425	958	12
RZ2439	S143	1	12 40 08.30	-11 38 17.18	2.184	-0.902	2.363	1037	12
RZ2474	–	4	12 40 07.67	-11 44 48.30	2.028	-7.422	7.694	1102	28

Table A1 – *continued* IDs, positions and velocities for the sample.

ID	Alt ID	Mask	R.A. (J2000)	Dec. (J2000)	X (arcmin)	Y (arcmin)	R_p (arcmin)	V_r kms^{-1}	σV_r kms^{-1}
(1)	(2)	(3)	(4)	(5)	(6)	(7)	(8)	(9)	(10)
RZ2475	–	4	12 40 07.68	-11 46 04.80	2.031	-8.697	8.931	1075	9
RZ2491	S059	3	12 40 07.49	-11 35 51.47	1.985	1.526	2.503	1162	12
RZ2493	S180	3	12 40 07.45	-11 36 13.12	1.975	1.165	2.293	897	32
RZ2502	S030	1	12 40 07.26	-11 36 44.65	1.928	0.639	2.031	1359	8
RZ2503	–	2	12 40 07.25	-11 40 25.42	1.924	-3.040	3.598	770	10
RZ2532	S177	2	12 40 06.75	-11 38 26.82	1.802	-1.064	2.093	1134	8
RZ2549	S487	1	12 40 06.32	-11 35 12.58	1.696	2.174	2.757	862	39
RZ2567	S142	3	12 40 05.90	-11 39 25.10	1.594	-2.035	2.585	1364	11
RZ2568	–	4	12 40 05.86	-11 46 03.00	1.583	-8.667	8.810	613	19
RZ2572	–	2	12 40 05.71	-11 42 18.06	1.545	-4.918	5.154	1176	13
RZ2593	–	4	12 40 05.27	-11 43 15.23	1.437	-5.870	6.044	1186	21
RZ2611	S235	3	12 40 04.93	-11 35 27.44	1.354	1.926	2.355	888	22
RZ2623	–	2	12 40 04.68	-11 40 53.74	1.292	-3.512	3.742	1113	18
RZ2637	S099	2	12 40 04.45	-11 40 18.53	1.234	-2.925	3.175	1106	11
RZ2658	–	4	12 40 03.76	-11 45 35.63	1.066	-8.210	8.279	1723	8
RZ2659	S512	4	12 40 03.73	-11 40 16.43	1.059	-2.891	3.079	1436	41
RZ2664	–	4	12 40 03.65	-11 43 05.47	1.039	-5.708	5.801	1295	15
RZ2672	–	4	12 40 03.55	-11 46 03.45	1.014	-8.674	8.733	299	12
RZ2687	–	4	12 40 03.31	-11 43 37.54	0.954	-6.242	6.315	912	16
RZ2694	S239	1	12 40 03.24	-11 34 06.79	0.939	3.270	3.402	1113	48
RZ2720	–	4	12 40 02.60	-11 40 29.50	0.780	-3.108	3.205	826	21
RZ2747	S382	4	12 40 02.20	-11 39 47.09	0.682	-2.401	2.497	1253	62
RZ2769	S373	4	12 40 01.69	-11 39 37.78	0.556	-2.246	2.314	1384	27
RZ2770	S171	4	12 40 01.68	-11 35 23.65	0.555	1.989	2.065	1403	30
RZ2790	–	2	12 40 01.39	-11 40 52.10	0.482	-3.485	3.518	898	20
RZ2796	S175	2	12 40 01.25	-11 40 07.71	0.449	-2.745	2.782	1115	19
RZ2829	–	4	12 40 00.64	-11 42 23.95	0.298	-5.016	5.025	958	32
RZ2830	–	4	12 40 00.66	-11 44 09.49	0.302	-6.775	6.782	1476	16
RZ2832	–	4	12 40 00.59	-11 44 55.97	0.286	-7.550	7.555	1122	8
RZ2835	S153	2	12 40 00.52	-11 39 52.63	0.270	-2.494	2.508	1400	13
RZ2847	S336	4	12 40 00.39	-11 39 05.47	0.236	-1.708	1.724	1278	18
RZ2862	–	4	12 40 00.11	-11 44 24.69	0.167	-7.028	7.030	1109	22
RZ2863	–	4	12 40 00.16	-11 32 27.71	0.180	4.921	4.925	1271	8
RZ2869	S222	1	12 40 00.04	-11 35 33.61	0.151	1.823	1.829	1190	14
RZ2883	S300	1	12 39 59.75	-11 35 29.14	0.080	1.898	1.899	1508	12
RZ2885	S138	4	12 39 59.71	-11 35 24.95	0.069	1.968	1.969	1257	18
RZ2915	S169	3	12 39 58.96	-11 35 44.10	-0.113	1.648	1.652	555	16
RZ2916	S015	4	12 39 58.94	-11 35 22.63	-0.118	2.006	2.010	1030	8
RZ2953	–	4	12 39 58.29	-11 33 18.06	-0.280	4.082	4.092	1259	17
RZ2967	S217	1	12 39 58.04	-11 35 30.83	-0.340	1.869	1.900	1144	9
RZ2968	S045	4	12 39 58.04	-11 34 26.75	-0.341	2.937	2.957	971	11
RZ2980	–	4	12 39 57.62	-11 41 15.10	-0.445	-3.868	3.894	1240	16
RZ2996	S137	4	12 39 57.48	-11 35 04.28	-0.478	2.312	2.361	1101	16
RZ3020	S104	4	12 39 56.83	-11 35 13.63	-0.636	2.156	2.248	951	10
RZ3026	–	4	12 39 56.71	-11 32 52.22	-0.668	4.513	4.562	885	25
RZ3027	–	4	12 39 56.66	-11 42 32.66	-0.681	-5.161	5.206	1183	19
RZ3029	–	2	12 39 56.63	-11 39 55.73	-0.688	-2.546	2.637	1166	21
RZ3057	–	4	12 39 56.00	-11 41 30.84	-0.844	-4.131	4.216	878	27
RZ3058	–	4	12 39 55.89	-11 42 28.72	-0.871	-5.095	5.169	1040	8
RZ3061	S011	4	12 39 55.83	-11 34 48.38	-0.883	2.577	2.724	995	8
RZ3075	–	1	12 39 55.44	-11 33 24.19	-0.981	3.980	4.099	1115	9
RZ3081	S174	4	12 39 55.36	-11 34 32.68	-1.000	2.839	3.010	1090	18
RZ3110	S165	1	12 39 54.60	-11 35 19.50	-1.187	2.058	2.376	939	8
RZ3160	S131	4	12 39 53.34	-11 39 52.22	-1.497	-2.487	2.903	1416	8
RZ3174	–	4	12 39 52.90	-11 30 59.40	-1.605	6.393	6.592	1087	34
RZ3191	S071	3	12 39 52.37	-11 35 40.44	-1.736	1.709	2.436	1098	14
RZ3193	–	1	12 39 52.26	-11 33 15.16	-1.763	4.131	4.491	1070	44
RZ3201	S048	2	12 39 52.16	-11 38 01.55	-1.787	-0.642	1.899	1209	8
RZ3218	S501	2	12 39 51.92	-11 38 24.33	-1.846	-1.022	2.110	1318	38
RZ3221	–	4	12 39 51.92	-11 32 22.43	-1.847	5.010	5.339	1034	21

Table A1 – *continued* IDs, positions and velocities for the sample.

ID	Alt ID	Mask	R.A. (J2000)	Dec. (J2000)	X (arcmin)	Y (arcmin)	R_p (arcmin)	V_r kms^{-1}	σV_r kms^{-1}
(1)	(2)	(3)	(4)	(5)	(6)	(7)	(8)	(9)	(10)
RZ3222	S026	1	12 39 51.88	-11 36 27.15	-1.854	0.930	2.075	1450	8
RZ3226	S112	4	12 39 51.80	-11 39 24.71	-1.876	-2.028	2.763	1149	8
RZ3236	S420	2	12 39 51.62	-11 36 07.66	-1.920	1.256	2.294	759	10
RZ3244	S084	2	12 39 51.51	-11 36 28.83	-1.946	0.902	2.145	1269	8
RZ3261	S433	2	12 39 51.24	-11 38 17.57	-2.013	-0.909	2.209	791	21
RZ3265	S028	3	12 39 51.16	-11 38 33.57	-2.034	-1.176	2.349	824	8
RZ3274	S073	3	12 39 50.99	-11 38 23.26	-2.075	-1.004	2.305	1184	15
RZ3283	S188	1	12 39 50.86	-11 36 07.09	-2.105	1.265	2.456	1105	8
RZ3319	S401	2	12 39 50.12	-11 38 04.26	-2.287	-0.687	2.389	1056	32
RZ3320	S013	3	12 39 50.13	-11 38 28.89	-2.288	-1.098	2.537	1314	8
RZ3354	S364	4	12 39 49.34	-11 37 57.18	-2.479	-0.569	2.544	1275	15
RZ3355	S310	2	12 39 49.34	-11 38 46.37	-2.480	-1.389	2.843	840	24
RZ3363	–	4	12 39 49.22	-11 32 08.87	-2.510	5.236	5.806	1168	40
RZ3396	S129	3	12 39 48.09	-11 38 02.49	-2.787	-0.658	2.864	703	11
RZ3398	–	4	12 39 48.07	-11 30 44.46	-2.793	6.642	7.206	1654	14
RZ3408	S294	2	12 39 47.83	-11 38 00.85	-2.851	-0.630	2.920	1110	17
RZ3431	S060	3	12 39 47.26	-11 38 08.23	-2.993	-0.753	3.086	1557	8
RZ3434	–	1	12 39 47.22	-11 33 33.56	-3.002	3.824	4.862	1053	27
RZ3441	S115	2	12 39 47.03	-11 36 05.73	-3.047	1.288	3.308	1065	8
RZ3486	S079	1	12 39 46.13	-11 35 36.59	-3.269	1.774	3.719	888	8
RZ3489	S203	4	12 39 46.10	-11 36 12.98	-3.278	1.167	3.479	1068	8
RZ3491	S503	3	12 39 46.08	-11 37 55.67	-3.283	-0.544	3.327	867	17
RZ3512	S172	3	12 39 45.48	-11 37 12.52	-3.429	0.174	3.434	1191	32
RZ3517	S008	2	12 39 45.29	-11 36 00.50	-3.475	1.375	3.737	872	8
RZ3528	S377	1	12 39 45.01	-11 35 19.07	-3.545	2.066	4.103	1178	13
RZ3564	S237	2	12 39 44.19	-11 38 25.03	-3.747	-1.033	3.886	1337	17
RZ3575	S083	2	12 39 44.07	-11 37 29.64	-3.775	-0.110	3.777	1134	10
RZ3592	S247	1	12 39 43.73	-11 35 02.67	-3.859	2.339	4.513	610	8
RZ3601	S345	3	12 39 43.50	-11 35 54.98	-3.915	1.467	4.181	1096	19
RZ3616	S352	3	12 39 43.19	-11 36 42.93	-3.993	0.668	4.048	1430	20
RZ3632	S159	4	12 39 42.89	-11 34 18.06	-4.066	3.083	5.103	1066	8
RZ3643	S276	2	12 39 42.70	-11 36 15.64	-4.113	1.123	4.264	1104	12
RZ3662	S483	2	12 39 42.19	-11 35 26.25	-4.238	1.946	4.663	1434	19
RZ3667	S176	1	12 39 42.14	-11 35 23.38	-4.251	1.994	4.696	912	9
RZ3680	S012	2	12 39 41.97	-11 38 27.10	-4.292	-1.068	4.423	1060	8
RZ3704	S415	2	12 39 41.55	-11 37 09.80	-4.396	0.220	4.401	1061	17
RZ3745	S155	3	12 39 40.84	-11 37 12.71	-4.570	0.172	4.573	783	13
RZ3799	–	3	12 39 39.73	-11 35 38.98	-4.845	1.734	5.146	986	25
RZ3835	–	2	12 39 38.91	-11 35 12.16	-5.046	2.181	5.497	1318	8
RZ3872	–	3	12 39 38.16	-11 34 22.56	-5.230	3.008	6.033	250	20
RZ3873	–	2	12 39 38.14	-11 38 38.53	-5.236	-1.258	5.385	874	9
RZ3903	–	3	12 39 37.56	-11 36 39.63	-5.378	0.723	5.426	1114	19
RZ3937	–	2	12 39 36.84	-11 34 45.63	-5.555	2.624	6.143	993	8
RZ3951	–	3	12 39 36.50	-11 33 42.20	-5.638	3.681	6.733	1273	11
RZ3960	–	3	12 39 36.28	-11 33 05.77	-5.692	4.288	7.126	763	19
RZ4029	–	2	12 39 34.63	-11 36 18.90	-6.098	1.069	6.191	88	10
RZ4040	–	2	12 39 34.39	-11 34 40.16	-6.156	2.715	6.728	1345	12
RZ4100	–	2	12 39 32.86	-11 35 54.64	-6.534	1.474	6.698	874	71
RZ4129	–	2	12 39 32.07	-11 35 35.46	-6.727	1.794	6.962	791	21
RZ4134	–	3	12 39 31.93	-11 34 06.66	-6.762	3.274	7.513	908	25
RZ4140	–	2	12 39 31.75	-11 36 47.10	-6.806	0.599	6.833	271	19
RZ4143	–	3	12 39 31.69	-11 35 18.37	-6.821	2.078	7.131	906	24
RZ4160	–	2	12 39 31.48	-11 33 55.44	-6.872	3.461	7.694	1176	10
RZ4206	–	2	12 39 30.18	-11 36 13.74	-7.192	1.156	7.285	960	9
RZ4283	–	2	12 39 28.45	-11 35 54.55	-7.617	1.476	7.759	373	33
RZ4301	–	2	12 39 27.85	-11 36 38.57	-7.765	0.742	7.801	210	23
RZ4367	–	2	12 39 26.49	-11 35 22.96	-8.100	2.002	8.343	143	19
RZ4495	–	3	12 39 22.94	-11 34 11.63	-8.972	3.192	9.522	939	34
RZ4662	–	3	12 39 18.95	-11 34 02.44	-9.952	3.345	10.500	925	33
S001	–	2	12 40 10.04	-11 38 20.71	2.610	-0.961	2.781	1328	8

Table A1 – *continued* IDs, positions and velocities for the sample.

ID	Alt ID	Mask	R.A. (J2000)	Dec. (J2000)	X (arcmin)	Y (arcmin)	R_p (arcmin)	V_r kms^{-1}	σV_r kms^{-1}
(1)	(2)	(3)	(4)	(5)	(6)	(7)	(8)	(9)	(10)
S003	–	4	12 40 00.09	-11 36 09.13	0.164	1.231	1.242	392	8
S004	–	2	12 40 14.59	-11 38 27.99	3.729	-1.083	3.883	999	8
S007	–	1	12 39 48.62	-11 35 40.63	-2.657	1.706	3.158	1410	8
S017	–	4	12 40 00.05	-11 35 52.92	0.155	1.501	1.509	622	10
S027	–	3	12 40 00.29	-11 37 54.80	0.212	-0.530	0.571	982	8
S032	–	3	12 40 12.18	-11 37 34.53	3.138	-0.192	3.143	906	15
S034	–	1	12 39 54.56	-11 36 39.54	-1.196	0.724	1.398	1161	8
S035	–	2	12 40 01.05	-11 37 57.02	0.399	-0.567	0.693	1173	8
S037	–	1	12 40 06.19	-11 36 10.31	1.663	1.212	2.058	686	8
S039	–	4	12 39 54.75	-11 36 25.84	-1.149	0.952	1.493	1097	8
S043	–	4	12 39 59.31	-11 38 27.89	-0.028	-1.081	1.082	931	10
S044	–	3	12 39 52.36	-11 38 46.85	-1.738	-1.397	2.230	1585	8
S050	–	1	12 40 03.21	-11 36 04.36	0.931	1.311	1.608	814	8
S051	–	3	12 39 56.44	-11 38 01.66	-0.734	-0.644	0.976	1309	8
S057	–	3	12 39 56.92	-11 38 19.82	-0.616	-0.947	1.130	1017	8
S062	–	1	12 39 54.64	-11 36 02.54	-1.178	1.341	1.785	1037	8
S065	–	1	12 39 54.07	-11 36 04.86	-1.317	1.302	1.852	996	8
S066	–	2	12 39 59.41	-11 36 31.92	-0.003	0.851	0.851	1107	8
S070	–	2	12 39 47.23	-11 37 47.94	-2.999	-0.415	3.028	990	11
S072	–	1	12 39 53.92	-11 35 55.20	-1.354	1.463	1.994	1314	8
S075	–	2	12 39 52.93	-11 35 54.75	-1.598	1.471	2.172	1264	8
S076	–	3	12 40 04.96	-11 36 21.40	1.361	1.027	1.705	1454	20
S080	–	3	12 39 53.64	-11 37 01.01	-1.423	0.366	1.469	1257	12
S085	–	2	12 39 56.74	-11 36 40.57	-0.660	0.707	0.967	841	8
S095	–	4	12 39 48.94	-11 37 39.87	-2.577	-0.281	2.593	932	9
S097	–	2	12 40 03.02	-11 38 45.85	0.884	-1.381	1.640	846	9
S102	–	3	12 40 04.18	-11 35 41.20	1.171	1.697	2.061	885	24
S106	–	1	12 39 54.04	-11 36 35.45	-1.325	0.792	1.544	787	8
S111	–	2	12 39 52.72	-11 38 23.35	-1.648	-1.006	1.931	861	10
S113	–	4	12 39 58.30	-11 37 07.86	-0.277	0.252	0.374	1086	17
S125	–	2	12 40 01.20	-11 38 46.09	0.437	-1.385	1.452	897	10
S128	–	4	12 40 02.20	-11 38 50.00	0.682	-1.450	1.602	789	15
S133	–	3	12 39 59.10	-11 36 20.27	-0.078	1.045	1.048	908	23
S145	–	3	12 40 01.58	-11 36 16.87	0.529	1.102	1.223	900	18
S146	–	1	12 39 51.64	-11 34 22.05	-1.914	3.016	3.572	936	12
S151	–	1	12 39 59.92	-11 36 53.77	0.120	0.487	0.501	1081	11
S152	–	1	12 40 00.62	-11 37 05.54	0.293	0.290	0.413	1182	8
S161	–	1	12 40 11.54	-11 37 04.96	2.979	0.300	2.994	1448	11
S162	–	4	12 40 01.83	-11 38 23.58	0.593	-1.010	1.171	1128	14
S163	–	3	12 39 55.92	-11 36 44.44	-0.862	0.642	1.075	1101	23
S182	–	1	12 39 58.93	-11 36 54.75	-0.122	0.470	0.486	1018	8
S185	–	2	12 40 04.69	-11 38 28.74	1.296	-1.096	1.697	750	10
S194	–	3	12 39 58.02	-11 37 59.58	-0.345	-0.609	0.700	1073	9
S200	–	4	12 39 55.81	-11 38 19.88	-0.888	-0.947	1.299	1060	14
S209	–	4	12 39 58.79	-11 36 27.61	-0.155	0.923	0.936	947	17
S219	–	4	12 39 56.84	-11 36 45.52	-0.635	0.624	0.891	543	37
S220	–	2	12 39 46.94	-11 37 13.64	-3.071	0.156	3.075	1582	16
S223	–	1	12 40 04.69	-11 36 43.60	1.297	0.656	1.454	731	15
S229	–	3	12 40 02.45	-11 35 55.59	0.744	1.457	1.636	1098	25
S232	–	1	12 39 56.78	-11 35 53.89	-0.650	1.485	1.621	1264	9
S242	–	2	12 39 46.82	-11 36 28.10	-3.100	0.915	3.232	737	9
S256	–	3	12 40 00.05	-11 38 27.73	0.155	-1.079	1.090	1166	17
S263	–	2	12 40 01.88	-11 38 04.41	0.603	-0.690	0.916	700	11
S272	–	3	12 39 55.91	-11 36 27.05	-0.865	0.932	1.272	821	22
S273	–	4	12 39 54.63	-11 37 58.69	-1.179	-0.594	1.320	1477	14
S278	–	4	12 39 58.42	-11 38 59.79	-0.245	-1.613	1.632	1145	9
S280	–	2	12 40 02.13	-11 37 00.90	0.665	0.368	0.759	1438	8
S311	–	2	12 40 01.59	-11 37 59.51	0.533	-0.608	0.809	1214	10
S318	–	3	12 40 07.21	-11 37 03.66	1.915	0.322	1.942	1011	21
S335	–	3	12 39 53.98	-11 38 52.15	-1.340	-1.486	2.001	1082	10

Table A1 – *continued* IDs, positions and velocities for the sample.

ID	Alt ID	Mask	R.A. (J2000)	Dec. (J2000)	X (arcmin)	Y (arcmin)	R_p (arcmin)	V_r kms^{-1}	σV_r kms^{-1}
(1)	(2)	(3)	(4)	(5)	(6)	(7)	(8)	(9)	(10)
S358	–	2	12 40 11.51	-11 39 18.11	2.974	-1.918	3.539	1120	12
S363	–	1	12 40 03.37	-11 36 31.16	0.971	0.864	1.300	1450	34
S368	–	1	12 40 05.39	-11 37 59.00	1.466	-0.600	1.584	1315	28
S369	–	4	12 39 59.75	-11 37 54.27	0.079	-0.521	0.527	1635	14
S370	–	1	12 39 51.27	-11 34 55.48	-2.006	2.459	3.173	1169	8
S376	–	3	12 40 10.47	-11 36 36.33	2.717	0.778	2.826	1433	18
S384	–	4	12 39 58.84	-11 38 11.39	-0.144	-0.806	0.819	990	22
S388	–	1	12 40 07.73	-11 38 14.33	2.043	-0.855	2.214	1224	15
S393	–	3	12 39 48.68	-11 35 39.54	-2.642	1.724	3.155	1448	20
S435	–	2	12 39 47.96	-11 36 58.39	-2.820	0.410	2.849	735	17
S438	–	3	12 40 13.73	-11 39 54.90	3.520	-2.531	4.336	817	21
S449	–	4	12 39 55.85	-11 39 58.24	-0.879	-2.587	2.733	896	24
S490	–	2	12 40 15.77	-11 39 04.91	4.021	-1.698	4.365	803	11
S502	–	3	12 40 10.77	-11 38 18.93	2.791	-0.932	2.942	1201	33
S529	–	1	12 40 03.53	-11 37 50.57	1.010	-0.459	1.110	2285	36
S600	–	2	12 39 41.37	-11 34 53.43	-4.439	2.493	5.091	1323	8
S605	–	2	12 39 58.33	-11 38 41.53	-0.269	-1.309	1.336	1066	24
S626	–	4	12 39 54.17	-11 38 13.60	-1.293	-0.843	1.544	1691	19

Table B1. IDs, magnitudes, colours, indices and metallicites for the GC candidate sample.

ID (1)	Alt ID (2)	V (3)	B-R (4)	CH (5)	$[Fe/H]_{CH}$ (6)	Mgb (7)	$[Fe/H]_{Mgb}$ (8)	Fe5270 (9)	$[Fe/H]_{5270}$ (10)	$[Fe/H]$ (11)
RZ1191	–	20.37	1.22	0.170 (0.007)	-0.515 (0.079)	0.064 (0.005)	-1.309 (0.073)	0.053 (0.004)	-1.007 (0.085)	-0.937 (0.045)
RZ1192	–	21.20	1.05	0.032 (0.009)	-2.090 (0.113)	0.040 (0.006)	-1.649 (0.080)	–	–	–
RZ1210	–	22.66	1.09	0.047 (–)	-1.918 (–)	0.026 (0.010)	-1.848 (0.149)	0.032 (0.011)	-1.434 (0.217)	-1.917 (–)
RZ1255	–	19.81	1.24	0.116 (0.006)	-1.131 (0.075)	0.086 (0.003)	-0.997 (0.049)	0.048 (0.003)	-1.108 (0.074)	-1.089 (0.038)
RZ1271	–	21.96	1.67	-0.320 (0.009)	-6.108 (0.102)	0.229 (0.007)	1.029 (0.103)	0.116 (0.006)	0.277 (0.127)	-1.444 (0.064)
RZ1290	–	22.35	0.97	-0.014 (0.013)	-2.615 (0.149)	-0.055 (0.017)	-2.995 (0.237)	-0.031 (0.011)	-2.717 (0.220)	-2.801 (0.118)
RZ1312	–	22.26	1.09	0.102 (–)	-1.291 (–)	0.058 (0.010)	-1.394 (0.140)	0.045 (0.007)	-1.169 (0.146)	-1.291 (–)
RZ1405	–	22.05	1.02	0.168 (–)	-0.537 (–)	0.022 (0.009)	-1.904 (0.132)	0.068 (0.009)	-0.701 (0.187)	-0.539 (–)
RZ1470	–	23.08	1.14	0.147 (–)	-0.777 (–)	-0.034 (–)	-2.698 (–)	-0.073 (0.009)	-3.573 (0.183)	-1.739 (–)
RZ1506	–	19.04	1.49	0.187 (0.007)	-0.320 (0.076)	0.264 (0.005)	1.525 (0.071)	0.093 (0.002)	-0.192 (0.050)	0.373 (0.038)
RZ1532	–	20.91	1.01	0.063 (0.008)	-1.736 (0.089)	0.023 (0.005)	-1.890 (0.065)	0.031 (0.004)	-1.455 (0.074)	-1.689 (0.044)
RZ1533	–	21.33	1.00	0.036 (0.009)	-2.044 (0.100)	–	–	–	– –	–
RZ1567	–	21.09	1.09	0.124 (0.009)	-1.040 (0.100)	0.045 (0.006)	-1.578 (0.085)	0.014 (0.005)	-1.801 (0.104)	-1.471 (0.056)
RZ1591	–	21.87	1.42	0.158 (0.009)	-0.651 (0.100)	0.157 (0.005)	0.009 (0.077)	0.057 (0.005)	-0.925 (0.100)	-0.564 (0.054)
RZ1632	–	21.06	1.10	0.184 (0.007)	-0.355 (0.080)	0.121 (0.004)	-0.501 (0.062)	0.057 (0.004)	-0.925 (0.075)	-0.593 (0.042)
RZ1638	–	19.56	1.55	0.211 (0.006)	-0.046 (0.073)	0.206 (0.003)	0.703 (0.047)	0.097 (0.003)	-0.110 (0.057)	0.132 (0.034)
RZ1661	–	21.32	1.25	0.225 (0.009)	0.113 (0.106)	0.104 (0.006)	-0.742 (0.092)	0.060 (0.005)	-0.864 (0.110)	-0.491 (0.059)
RZ1690	–	21.80	1.43	0.260 (0.009)	0.513 (0.105)	0.138 (0.007)	-0.260 (0.105)	0.098 (0.008)	-0.090 (0.172)	0.030 (0.075)
RZ1724	–	21.80	1.46	0.144 (0.009)	-0.811 (0.107)	0.062 (0.006)	-1.337 (0.092)	–	–	–
RZ1733	–	20.71	1.05	0.051 (0.009)	-1.873 (0.098)	–	–	0.019 (0.005)	-1.699 (0.095)	–
RZ1771	–	20.82	1.26	0.177 (0.009)	-0.435 (0.100)	0.093 (0.005)	-0.898 (0.085)	0.021 (0.006)	-1.658 (0.116)	-1.037 (0.058)
RZ1780	–	22.02	1.42	0.414 (0.008)	2.271 (0.092)	–	–	0.069 (0.007)	-0.681 (0.137)	–
RZ1836	–	19.65	1.35	0.149 (0.006)	-0.754 (0.074)	0.105 (0.003)	-0.728 (0.049)	–	–	–
RZ1841	–	23.32	1.15	-0.390 (–)	-6.907 (–)	–	–	–	–	–
RZ1923	S366	22.21	1.46	0.024 (0.011)	-2.181 (0.127)	–	–	0.095 (0.006)	-0.151 (0.142)	–
RZ1934	–	20.23	1.24	0.120 (0.008)	-1.085 (0.089)	0.083 (0.003)	-1.040 (0.047)	–	–	–
RZ1946	S214	21.45	1.04	-0.004 (0.011)	-2.501 (0.125)	0.065 (0.007)	-1.295 (0.095)	–	–	–
RZ1983	S228	21.49	1.64	0.193 (0.008)	-0.252 (0.096)	0.251 (–)	1.341 (–)	0.100 (0.005)	-0.049 (0.112)	–
RZ1990	S230	21.56	1.35	0.055 (0.012)	-1.827 (0.143)	–	–	-0.005 (0.006)	-2.188 (0.129)	–
RZ1997	S204	21.50	1.21	0.164 (0.009)	-0.583 (0.105)	–	–	0.006 (0.006)	-1.964 (0.130)	–
RZ1998	–	20.55	1.61	0.122 (0.008)	-1.062 (0.091)	0.215 (0.006)	0.831 (0.089)	0.101 (0.003)	-0.029 (0.062)	-0.101 (0.047)
RZ2014	S271	21.74	1.29	0.289 (0.010)	0.844 (0.110)	0.142 (0.006)	-0.204 (0.088)	0.047 (0.006)	-1.129 (0.116)	-0.179 (0.060)
RZ2021	S047	20.18	1.15	0.066 (0.008)	-1.702 (0.096)	0.062 (0.004)	-1.337 (0.060)	0.025 (0.004)	-1.577 (0.073)	-1.567 (0.045)
RZ2024	–	20.05	1.26	0.186 (0.006)	-0.332 (0.064)	0.185 (0.003)	0.406 (0.047)	0.063 (0.002)	-0.803 (0.053)	-0.269 (0.031)
RZ2037	S236	21.67	1.15	-0.004 (0.011)	-2.501 (0.122)	–	–	0.027 (0.006)	-1.536 (0.127)	–
RZ2038	S009	19.38	1.30	0.109 (0.005)	-1.211 (0.061)	0.074 (0.002)	-1.167 (0.034)	–	–	–
RZ2055	–	21.37	1.20	0.098 (0.008)	-1.336 (0.095)	0.098 (0.004)	-0.827 (0.069)	0.036 (0.005)	-1.353 (0.097)	-1.206 (0.050)
RZ2059	S211	21.57	1.44	0.121 (0.009)	-1.074 (0.107)	0.123 (0.005)	-0.473 (0.074)	0.063 (0.004)	-0.803 (0.090)	-0.818 (0.052)
RZ2082	–	21.69	1.08	0.094 (0.010)	-1.382 (0.119)	0.083 (0.005)	-1.040 (0.080)	0.038 (0.005)	-1.312 (0.106)	-1.267 (0.059)
RZ2084	S197	21.44	1.17	0.085 (0.011)	-1.485 (0.122)	0.045 (0.007)	-1.578 (0.099)	0.035 (0.006)	-1.373 (0.122)	-1.472 (0.066)
RZ2106	S195	21.58	1.39	0.149 (0.010)	-0.754 (0.111)	0.103 (0.006)	-0.756 (0.091)	–	–	–
RZ2109	S077	20.59	1.38	0.142 (0.008)	-0.834 (0.090)	0.116 (0.005)	-0.572 (0.072)	0.054 (0.004)	-0.986 (0.086)	-0.811 (0.048)
RZ2144	S021	19.77	1.20	0.106 (0.006)	-1.245 (0.065)	–	–	0.035 (0.002)	-1.373 (0.048)	–
RZ2194	–	21.51	1.15	0.056 (0.009)	-1.816 (0.102)	0.050 (0.005)	-1.507 (0.078)	0.052 (0.005)	-1.027 (0.100)	-1.448 (0.054)
RZ2237	–	20.54	1.18	0.064 (0.011)	-1.724 (0.123)	0.098 (0.007)	-0.827 (0.099)	0.040 (0.006)	-1.271 (0.128)	-1.305 (0.067)
RZ2242	S063	20.41	1.07	0.018 (0.006)	-2.250 (0.070)	0.013 (0.004)	-2.032 (0.054)	0.012 (0.003)	-1.842 (0.063)	-2.051 (0.036)
RZ2276	S234	21.69	1.62	0.624 (0.008)	4.668 (0.090)	–	–	0.142 (0.006)	0.806 (0.129)	–
RZ2289	S069	20.49	1.04	-0.006 (0.010)	-2.523 (0.109)	0.001 (0.005)	-2.202 (0.070)	0.018 (0.004)	-1.719 (0.081)	-2.186 (0.050)
RZ2303	S033	19.98	1.18	0.057 (0.007)	-1.804 (0.080)	–	–	–	–	–
RZ2305	S248	21.73	1.45	0.113 (0.009)	-1.165 (0.107)	–	–	0.061 (0.005)	-0.844 (0.107)	–
RZ2307	S055	20.31	1.49	0.172 (0.010)	-0.492 (0.119)	0.110 (0.004)	-0.657 (0.063)	0.062 (0.004)	-0.823 (0.074)	-0.628 (0.051)
RZ2316	–	20.31	1.41	0.162 (0.011)	-0.606 (0.126)	0.135 (0.008)	-0.303 (0.110)	0.064 (0.007)	-0.783 (0.133)	-0.579 (0.071)
RZ2342	–	21.55	1.05	-0.032 (0.008)	-2.820 (0.088)	0.082 (0.005)	-1.054 (0.071)	0.001 (0.005)	-2.066 (0.097)	-2.045 (0.049)
RZ2344	–	21.28	1.35	0.065 (0.011)	-1.713 (0.124)	0.075 (0.010)	-1.153 (0.141)	0.041 (0.008)	-1.251 (0.160)	-1.353 (0.082)
RZ2363	S016	19.43	1.21	0.088 (0.006)	-1.450 (0.072)	0.060 (0.003)	-1.366 (0.045)	–	–	–
RZ2381	S019	19.83	1.33	0.113 (0.007)	-1.165 (0.081)	0.116 (0.004)	-0.572 (0.054)	0.050 (0.003)	-1.068 (0.066)	-0.974 (0.039)
RZ2390	S492	22.62	1.43	1.548 (0.016)	15.220 (0.179)	0.149 (0.011)	-0.105 (0.155)	-0.003 (0.008)	-2.147 (0.160)	–
RZ2410	S093	20.78	1.19	0.007 (0.010)	-2.375 (0.115)	0.074 (0.006)	-1.167 (0.081)	0.040 (0.005)	-1.271 (0.107)	-1.661 (0.059)
RZ2428	–	20.38	1.11	0.114 (0.005)	-1.154 (0.061)	0.049 (0.008)	-1.522 (0.116)	0.032 (0.009)	-1.434 (0.177)	-1.415 (0.073)
RZ2439	S143	21.17	1.10	0.085 (0.009)	-1.485 (0.109)	-0.011 (0.007)	-2.372 (0.102)	0.031 (0.006)	-1.455 (0.115)	-1.752 (0.062)

Table B1 – *continued* IDs, magnitudes, colours, indices and metallicites for the sample.

ID (1)	Alt ID (2)	V (3)	B-R (4)	CH (5)	[Fe/H]$_{CH}$ (6)	Mgb (7)	[Fe/H]$_{Mgb}$ (8)	Fe5270 (9)	[Fe/H]$_{5270}$ (10)	[Fe/H] (11)
RZ2475	–	20.02	1.19	0.090 (0.010)	-1.428 (0.111)	0.052 (0.008)	-1.479 (0.106)	– –	–	–
RZ2491	S059	20.44	1.29	0.120 (0.008)	-1.085 (0.095)	0.066 (0.005)	-1.281 (0.066)	0.032 (0.004)	-1.434 (0.080)	-1.255 (0.046)
RZ2493	S180	21.39	1.21	0.016 (0.011)	-2.272 (0.130)	-0.017 (0.007)	-2.457 (0.097)	0.053 (0.005)	-1.007 (0.106)	-1.923 (0.064)
RZ2502	S030	19.93	1.42	0.198 (0.006)	-0.195 (0.075)	0.139 (0.004)	-0.246 (0.052)	0.079 (0.003)	-0.477 (0.071)	-0.309 (0.038)
RZ2503	–	20.28	1.28	0.134 (0.006)	-0.925 (0.074)	0.088 (0.003)	-0.969 (0.047)	0.043 (0.003)	-1.210 (0.063)	-1.033 (0.036)
RZ2532	S177	21.48	1.24	0.291 (0.012)	0.867 (0.134)	–	–	0.040 (0.005)	-1.271 (0.096)	–
RZ2549	S487	22.57	1.07	-0.290 (–)	-5.765 (–)	–	–	–	–	–
RZ2567	S142	21.16	1.13	0.102 (0.009)	-1.291 (0.101)	0.026 (0.007)	-1.848 (0.093)	0.038 (0.005)	-1.312 (0.108)	-1.470 (0.058)
RZ2572	–	20.91	1.14	0.120 (0.009)	-1.085 (0.099)	0.036 (0.005)	-1.706 (0.072)	0.042 (0.004)	-1.231 (0.084)	-1.308 (0.049)
RZ2593	–	22.27	1.56	0.239 (0.010)	0.273 (0.116)	0.246 (0.008)	1.270 0.111)	0.029 (–)	-1.495 (–)	-1.490 (–)
RZ2611	S235	21.70	1.44	0.093 (0.010)	-1.393 (0.116)	0.051 (0.008)	-1.493 (0.108)	0.012 (0.006)	-1.842 (0.124)	-1.584 (0.067)
RZ2623	–	21.64	1.39	0.138 (0.009)	-0.880 (0.101)	0.076 (0.005)	-1.139 (0.075)	0.057 (0.005)	-0.925 (0.096)	-0.967 (0.052)
RZ2637	S099	20.84	1.49	0.061 (0.007)	-1.759 (0.085)	0.062 (0.006)	-1.337 (0.085)	–	–	–
RZ2658	–	20.62	1.12	0.092 (–)	-1.405 (–)	–	–	–	–	-1.213 (–)
RZ2664	–	21.59	1.20	0.221 (0.009)	0.068 (0.103)	0.071 (0.007)	-1.210 (0.097)	–	–	–
RZ2687	–	21.49	1.12	0.165 (–)	-0.572 (–)	0.063 (–)	-1.323 (–)	–	–	–
RZ2694	S239	21.67	1.07	-0.092 (0.016)	-3.505 (0.182)	0.061 (0.008)	-1.352 (0.108)	0.070 (0.006)	-0.660 (0.122)	-2.102 (0.081)
RZ2720	–	21.77	1.11	0.058 (0.009)	-1.793 (0.105)	0.065 (–)	-1.295 (–)	0.022 (–)	-1.638 (–)	-1.467 (–)
RZ2747	S382	22.27	1.42	0.223 (–)	0.091 (–)	0.198 (0.016)	0.590 (0.229)	0.053 (0.008)	-1.007 (0.160)	0.090 (–)
RZ2769	S373	22.18	1.51	0.274 (0.009)	0.673 (0.106)	0.104 (0.009)	-0.742 (0.134)	0.018 (0.008)	-1.719 (0.168)	-0.776 (0.079)
RZ2770	S171	21.23	1.08	0.035 (0.010)	-2.055 (0.112)	0.000 (0.008)	-2.216 (0.107)	-0.009 (0.006)	-2.269 (0.116)	-2.181 (0.064)
RZ2790	–	22.29	1.38	0.350 (0.009)	1.540 (0.104)	0.153 (0.006)	-0.048 (0.091)	0.080 (0.006)	-0.457 (0.122)	0.316 (0.061)
RZ2796	S175	21.33	1.14	-0.004 (0.008)	-2.501 (0.093)	0.025 (0.005)	-1.862 (0.070)	0.007 (0.004)	-1.943 (0.085)	-2.129 (0.048)
RZ2830	–	21.59	1.14	0.200 (0.007)	-0.172 (0.085)	–	–	–	–	–
RZ2832	–	19.77	1.52	0.215 (0.013)	0.001 (0.146)	–	–	–	–	–
RZ2835	S153	21.24	1.26	0.077 (0.008)	-1.576 (0.097)	0.064 (0.005)	-1.309 (0.066)	0.046 (0.004)	-1.149 (0.078)	-1.365 (0.047)
RZ2847	S336	22.06	1.56	0.255 (0.009)	0.456 (0.104)	0.091 (0.008)	-0.926 (0.119)	0.027 (0.007)	-1.536 (0.150)	-0.786 (0.072)
RZ2862	–	21.49	1.06	-0.107 (0.014)	-3.676 (0.163)	–	–	–	–	–
RZ2863	–	19.36	1.39	0.125 (0.008)	-1.028 (0.087)	0.088 (0.008)	-0.969 (0.114)	0.046 (0.008)	-1.149 (0.158)	-1.063 (0.071)
RZ2869	S222	21.59	1.18	0.170 (0.009)	-0.515 (0.105)	0.086 (0.007)	-0.997 (0.094)	–	–	–
RZ2883	S300	21.84	1.40	-0.096 (–)	-3.551 (–)	0.066 (0.008)	-1.281 (0.111)	–	–	–
RZ2885	S138	21.10	1.41	0.045 (0.011)	-1.941 (0.122)	0.123 (0.006)	-0.473 (0.089)	0.042 (0.006)	-1.231 (0.116)	-1.290 (0.063)
RZ2915	S169	21.34	1.17	-0.039 (0.014)	-2.900 (0.157)	0.047 (0.006)	-1.550 (0.092)	0.043 (0.007)	-1.210 (0.137)	-1.978 (0.075)
RZ2916	S015	19.49	1.27	0.123 (0.007)	-1.051 (0.075)	0.077 (0.004)	-1.125 (0.053)	0.034 (0.003)	-1.394 (0.068)	-1.190 (0.038)
RZ2953	–	21.12	1.17	-0.029 (–)	-2.786 (–)	-0.015 (–)	-2.429 (–)	0.038 (–)	-1.312 (–)	-2.176 (–)
RZ2967	S217	21.61	1.14	0.041 (0.010)	-1.987 (0.117)	-0.045 (0.008)	-2.854 (0.116)	–	–	–
RZ2968	S045	20.27	1.49	0.154 (0.008)	-0.697 (0.090)	0.146 (0.005)	-0.147 (0.066)	0.079 (0.005)	-0.477 (0.098)	-0.469 (0.049)
RZ2980	–	22.06	1.69	0.306 (0.009)	1.038 (0.105)	– –	–	0.133 (0.008)	0.623 (0.155)	–
RZ2996	S137	21.14	1.09	-0.003 (0.010)	-2.489 (0.110)	0.053 (0.006)	-1.465 (0.091)	0.036 (0.005)	-1.353 (0.109)	-1.789 (0.059)
RZ3020	S104	20.87	1.44	0.104 (0.011)	-1.268 (0.120)	0.093 (0.006)	-0.898 (0.085)	0.060 (0.005)	-0.864 (0.101)	-1.032 (0.059)
RZ3026	–	22.03	1.48	0.422 (0.011)	2.362 (0.130)	0.139 (–)	-0.246 (–)	0.014 (–)	-1.801 (–)	-1.021 (–)
RZ3027	–	22.58	1.08	-0.137 (0.013)	-4.019 (0.149)	–	–	–	–	–
RZ3029	–	22.11	1.00	0.024 (0.009)	-2.181 (0.108)	0.036 (0.007)	-1.706 (0.093)	0.003 (0.006)	-2.025 (0.112)	-1.984 (0.060)
RZ3057	–	22.07	1.18	0.223 (0.008)	0.091 (0.093)	–	–	–	–	–
RZ3058	–	21.47	1.12	0.005 (0.010)	-2.398 (0.113)	0.035 (0.007)	-1.720 (0.098)	0.041 (0.006)	-1.251 (0.123)	-1.777 (0.064)
RZ3061	S011	19.45	1.59	0.152 (0.006)	-0.720 (0.072)	0.187 (0.004)	0.434 (0.053)	0.086 (0.003)	-0.334 (0.069)	-0.267 (0.037)
RZ3075	–	19.81	1.19	0.073 (0.007)	-1.622 (0.080)	0.051 (0.004)	-1.493 (0.058)	0.022 (0.003)	-1.638 (0.068)	-1.591 (0.039)
RZ3081	S174	21.30	1.11	0.084 (0.010)	-1.496 (0.118)	0.073 (0.007)	-1.182 (0.093)	0.025 (0.006)	-1.577 (0.128)	-1.440 (0.065)
RZ3110	S165	21.36	1.56	0.382 (0.008)	1.906 (0.089)	–	–	0.078 (0.005)	-0.497 (0.112)	–
RZ3160	S131	21.00	1.22	0.192 (0.008)	-0.263 (0.095)	0.057 (0.006)	-1.408 (0.092)	0.037 (0.005)	-1.332 (0.111)	-1.015 (0.057)
RZ3174	–	21.44	1.42	0.330 (0.011)	1.312 (0.131)	0.117 (–)	-0.558 (–)	0.075 (–)	-0.558 (–)	-0.557 (–)
RZ3191	S071	20.47	1.48	0.107 (0.011)	-1.234 (0.129)	0.100 (0.006)	-0.799 (0.086)	0.042 (0.005)	-1.231 (0.092)	-1.111 (0.060)
RZ3193	–	22.80	1.58	0.259 (0.010)	0.502 (0.117)	–	–	0.121 (0.008)	0.378 (0.169)	–
RZ3201	S048	20.27	1.44	0.181 (0.006)	-0.389 (0.069)	0.127 (0.003)	-0.416 (0.047)	0.058 (–)	-0.905 (–)	-0.904 (–)
RZ3218	S501	22.65	1.13	-0.007 (0.013)	-2.535 (0.148)	0.027 (0.008)	-1.833 (0.119)	0.012 (0.008)	-1.842 (0.159)	-2.079 (0.082)
RZ3221	–	21.30	1.29	0.059 (0.012)	-1.782 (0.133)	0.079 (0.008)	-1.096 (0.120)	0.025 (0.010)	-1.577 (0.204)	-1.510 (0.090)
RZ3222	S026	19.91	1.35	0.133 (0.007)	-0.937 (0.077)	0.070 (0.004)	-1.224 (0.052)	0.053 (0.003)	-1.007 (0.062)	-1.038 (0.037)
RZ3226	S112	20.94	1.39	0.143 (0.008)	-0.823 (0.095)	0.096 (0.006)	-0.856 (0.092)	0.079 (0.005)	-0.477 (0.112)	-0.703 (0.057)
RZ3236	S420	22.39	1.23	0.085 (0.009)	-1.485 (0.105)	0.038 (0.008)	-1.678 (0.115)	0.036 (0.007)	-1.353 (0.137)	-1.497 (0.069)
RZ3244	S084	20.78	1.53	0.172 (0.007)	-0.492 (0.080)	0.117 (0.004)	-0.558 (0.060)	0.066 (0.004)	-0.742 (0.071)	-0.595 (0.041)

Table B1 – *continued* IDs, magnitudes, colours, indices and metallicites for the sample.

ID (1)	Alt ID (2)	V (3)	B-R (4)	CH (5)	[Fe/H]$_{CH}$ (6)	Mgb (7)	[Fe/H]$_{Mgb}$ (8)	Fe5270 (9)	[Fe/H]$_{5270}$ (10)	[Fe/H] (11)
RZ3261	S433	22.46	1.20	0.019 (0.011)	-2.238 (0.122)	0.025 (0.008)	-1.862 (0.108)	0.029 (0.006)	-1.495 (0.132)	-1.856 (0.070)
RZ3265	S028	19.96	1.59	0.154 (0.007)	-0.697 (0.080)	0.183 (0.004)	0.377 (0.058)	0.072 (0.004)	-0.620 (0.072)	-0.374 (0.040)
RZ3274	S073	20.69	1.21	0.077 (0.008)	-1.576 (0.092)	0.047 (−)	-1.550 (−)	-0.012 (−)	-2.330 (−)	-1.940 (−)
RZ3283	S188	21.44	1.18	0.264 (0.008)	0.559 (0.091)	−	−	0.027 (0.006)	-1.536 (0.114)	−
RZ3319	S401	22.42	1.13	0.056 (−)	-1.816 (−)	0.089 (0.008)	-0.955 (0.111)	0.074 (0.007)	-0.579 (0.141)	-1.813 (−)
RZ3320	S013	19.50	1.46	0.163 (0.007)	-0.594 (0.077)	0.104 (0.004)	-0.742 (0.056)	0.056 (0.003)	-0.945 (0.064)	-0.750 (0.038)
RZ3354	S364	22.16	1.20	0.062 (0.010)	-1.747 (0.115)	0.065 (0.010)	-1.295 (0.135)	0.036 (0.009)	-1.353 (0.174)	-1.441 (0.082)
RZ3355	S310	22.00	1.24	0.096 (0.010)	-1.359 (0.118)	0.074 (0.006)	-1.167 (0.088)	0.052 (0.005)	-1.027 (0.105)	-1.193 (0.060)
RZ3363	−	22.39	1.54	0.331 (0.013)	1.323 (0.150)	0.297 (−)	1.993 (−)	−	−	−
RZ3396	S129	21.04	1.09	0.126 (0.009)	-1.017 (0.100)	0.018 (0.006)	-1.961 (0.088)	0.017 (0.005)	-1.740 (0.108)	-1.561 (0.057)
RZ3398	−	21.98	1.05	0.057 (0.009)	-1.804 (0.108)	0.035 (−)	-1.720 (−)	−	−	−
RZ3408	S294	21.91	1.47	0.158 (0.011)	-0.651 (0.132)	0.143 (0.006)	-0.190 (0.089)	0.064 (0.005)	-0.783 (0.109)	-0.569 (0.064)
RZ3431	S060	20.45	1.18	0.079 (0.008)	-1.553 (0.093)	0.024 (0.006)	-1.876 (0.090)	0.024 (0.005)	-1.597 (0.093)	-1.673 (0.053)
RZ3434	−	22.20	1.48	0.486 (0.014)	3.093 (0.159)	0.184 (0.007)	0.391 (0.103)	−	−	−
RZ3441	S115	20.94	1.19	0.114 (0.008)	-1.154 (0.094)	0.066 (0.005)	-1.281 (0.065)	0.065 (0.004)	-0.762 (0.076)	-1.062 (0.045)
RZ3486	S079	20.66	1.54	0.246 (0.007)	0.353 (0.084)	0.161 (0.006)	0.066 (0.082)	0.079 (0.004)	-0.477 (0.083)	-0.017 (0.048)
RZ3489	S203	21.36	1.49	0.184 (0.009)	-0.355 (0.105)	0.149 (0.007)	-0.105 (0.099)	0.030 (0.006)	-1.475 (0.128)	-0.712 (0.064)
RZ3491	S503	22.69	1.44	-0.126 (−)	-3.893 (−)	0.253 (0.008)	1.369 (0.115)	0.000 (0.009)	-2.086 (0.177)	-3.884 (−)
RZ3512	S172	21.30	1.10	-0.022 (0.010)	-2.706 (0.111)	−	−	−	−	−
RZ3517	S008	19.28	1.54	0.189 (0.005)	-0.298 (0.054)	0.162 (0.002)	0.080 (0.033)	0.075 (0.002)	-0.558 (0.040)	-0.281 (0.024)
RZ3528	S377	22.26	1.43	0.418 (0.008)	2.316 (0.091)	0.133 (0.008)	-0.331 (0.109)	0.086 (0.009)	-0.334 (0.179)	0.303 (0.076)
RZ3564	S237	21.78	1.32	0.116 (0.011)	-1.131 (0.130)	0.107 (0.006)	-0.700 (0.079)	0.034 (0.005)	-1.394 (0.101)	-1.107 (0.061)
RZ3575	S083	20.69	1.38	0.111 (0.007)	-1.188 (0.085)	0.089 (0.004)	-0.955 (0.056)	0.039 (0.003)	-1.292 (0.070)	-1.161 (0.041)
RZ3592	S247	21.75	1.33	0.234 (0.008)	0.216 (0.095)	−	−	0.029 (0.006)	-1.495 (0.121)	−
RZ3601	S345	22.09	1.43	0.266 (0.011)	0.581 (0.125)	0.101 (0.008)	-0.785 (0.120)	0.063 (0.006)	-0.803 (0.132)	-0.338 (0.072)
RZ3616	S352	22.14	1.19	0.019 (0.011)	-2.238 (0.125)	0.022 (0.008)	-1.904 (0.112)	−	−	−
RZ3632	S159	21.31	1.15	-0.025 (0.014)	-2.740 (0.164)	0.088 (0.007)	-0.969 (0.101)	0.018 (0.006)	-1.719 (0.126)	-1.954 (0.076)
RZ3643	S276	21.86	1.20	0.067 (0.010)	-1.690 (0.125)	−	−	0.035 (0.006)	-1.373 (0.120)	−
RZ3662	S483	22.64	1.00	-0.125 (0.015)	-3.882 (0.174)	−	−	−	−	−
RZ3667	S176	21.34	1.40	0.209 (0.009)	-0.069 (0.101)	−	−	−	−	−
RZ3680	S012	19.47	1.19	0.080 (0.006)	-1.542 (0.065)	0.052 (0.002)	-1.479 (0.036)	0.030 (0.002)	-1.475 (0.044)	-1.506 (0.028)
RZ3704	S415	22.44	1.37	0.349 (0.009)	1.529 (−)	0.137 (0.007)	-0.275 (0.101)	0.072 (0.007)	-0.620 (0.141)	0.110 (0.066)
RZ3745	S155	21.23	1.03	-0.009 (0.011)	-2.558 (0.121)	−	−	0.013 (1.763)	-1.821 (−)	−
RZ3799	−	22.28	1.50	0.251 (−)	0.410 (−)	0.053 (−)	-1.465 (−)	0.091 (−)	-0.233 (−)	-0.429 (−)
RZ3835	−	20.47	1.12	0.039 (0.006)	-2.010 (0.073)	0.027 (0.004)	-1.833 (0.057)	0.032 (0.003)	-1.434 (0.066)	-1.765 (0.037)
RZ3872	−	21.53	1.11	0.151 (0.009)	-0.731 (0.099)	0.096 (−)	-0.856 (−)	0.029 (−)	-1.495 (−)	-1.175 (−)
RZ3873	−	20.16	1.15	0.103 (0.006)	-1.279 (0.068)	0.030 (0.003)	-1.791 (0.048)	0.022 (0.003)	-1.638 (0.055)	-1.538 (0.033)
RZ3903	−	21.14	1.17	0.093 (0.008)	-1.393 (0.095)	−	−	0.018 (0.004)	-1.719 (0.084)	−
RZ3937	−	21.77	1.29	0.280 (0.008)	0.741 (0.094)	0.089 (0.007)	-0.955 (0.094)	0.073 (0.005)	-0.599 (0.111)	-0.289 (0.057)
RZ3951	−	20.61	0.93	0.104 (0.008)	-1.268 (0.097)	0.005 (0.005)	-2.145 (0.075)	0.014 (0.005)	-1.801 (0.096)	-1.704 (0.051)
RZ3960	−	20.56	1.37	0.206 (0.013)	-0.104 (0.148)	0.077 (0.007)	-1.125 (0.099)	0.054 (0.006)	-0.986 (0.122)	-0.669 (0.071)
RZ4029	−	20.77	1.30	0.186 (0.007)	-0.332 (0.083)	0.137 (0.004)	-0.275 (0.061)	0.025 (0.970)	-1.577 (−)	-1.575 (−)
RZ4040	−	22.35	1.19	0.009 (0.010)	-2.352 (0.117)	−	−	−	−	−
RZ4100	−	21.85	1.07	-0.010 (0.010)	-2.569 (0.109)	0.047 (0.006)	-1.550 (0.082)	−	−	−
RZ4129	−	22.27	1.42	0.393 (0.009)	2.031 (0.103)	0.159 (0.007)	0.037 (0.095)	0.068 (0.006)	-0.701 (0.126)	0.383 (0.062)
RZ4134	−	22.02	1.56	0.211 (−)	-0.046 (−)	0.140 (0.011)	-0.232 (0.162)	0.068 (−)	-0.701 (−)	-0.373 (−)
RZ4140	−	21.70	1.04	0.157 (0.008)	-0.663 (0.090)	0.105 (0.005)	-0.728 (0.076)	0.036 (0.005)	-1.353 (0.094)	-0.931 (0.050)
RZ4143	−	23.17	1.78	-0.210 (−)	-4.852 (−)	0.219 (0.011)	0.887 (0.159)	−	−	-4.734 (−)
RZ4160	−	21.14	1.09	0.080 (0.008)	-1.542 (0.089)	0.019 (0.005)	-1.947 (0.075)	0.017 (0.004)	-1.740 (0.090)	-1.732 (0.049)
RZ4206	−	19.71	1.16	0.098 (0.006)	-1.336 (0.066)	0.045 (0.003)	-1.578 (0.040)	0.035 (0.003)	-1.373 (0.052)	-1.409 (0.031)
RZ4283	−	23.17	1.41	0.015 (−)	-2.284 (−)	0.183 (0.008)	0.377 (0.115)	0.095 (0.007)	-0.151 (0.151)	-2.278 (—)
RZ4301	−	20.73	1.09	0.107 (0.007)	-1.234 (0.074)	0.066 (0.004)	-1.281 (0.052)	0.007 (0.003)	-1.943 (0.071)	-1.502 (0.038)
RZ4367	−	21.69	1.41	0.050 (0.010)	-1.884 (0.112)	0.144 (0.006)	-0.175 (0.083)	−	−	−
RZ4495	−	22.10	1.31	-0.084 (−)	-3.414 (−)	0.048 (−)	-1.536 (−)	0.049 (−)	-1.088 (−)	-2.013 (−)
RZ4662	−	21.46	1.34	0.121 (−)	-1.074 (−)	0.057 (−)	-1.408 (−)	0.026 (−)	-1.556 (−)	-1.346 (−)
S001	−	18.74	1.26	0.115 (0.004)	-1.142 (0.047)	0.065 (0.002)	-1.295 (0.031)	0.045 (0.002)	-1.169 (0.035)	-1.192 (0.022)
S003	−	18.83	1.27	0.117 (0.005)	-1.119 (0.061)	0.065 (0.003)	-1.295 (0.042)	0.046 (0.002)	-1.149 (0.049)	-1.177 (0.029)
S004	−	18.83	1.36	0.154 (0.004)	-0.697 (0.049)	0.089 (0.002)	-0.955 (0.030)	0.050 (0.002)	-1.068 (0.035)	-0.879 (0.022)
S007	−	19.04	1.31	0.100 (0.005)	-1.314 (0.060)	0.083 (0.003)	-1.040 (0.041)	0.049 (0.003)	-1.088 (0.068)	-1.157 (0.033)
S017	−	19.64	1.23	0.096 (0.008)	-1.359 (0.097)	0.073 (0.004)	-1.182 (0.064)	0.033 (0.004)	-1.414 (0.078)	-1.330 (0.046)

Table B1 – *continued* IDs, magnitudes, colours, indices and metallicites for the sample.

ID (1)	Alt ID (2)	V (3)	B-R (4)	CH (5)	[Fe/H]$_{CH}$ (6)	Mgb (7)	[Fe/H]$_{Mgb}$ (8)	Fe5270 (9)	[Fe/H]$_{5270}$ (10)	[Fe/H] (11)
S027	–	19.92	1.25	0.112 (0.007)	-1.177 (0.078)	0.063 (0.004)	-1.323 (0.057)	–	–	–
S032	–	19.95	1.35	0.040 (0.008)	-1.998 (0.090)	0.039 (0.004)	-1.663 (0.062)	0.006 (0.004)	-1.964 (0.075)	-1.895 (0.044)
S034	–	20.03	1.22	0.068 (0.008)	-1.679 (0.087)	0.074 (0.004)	-1.167 (0.059)	0.051 (0.003)	-1.047 (0.069)	-1.337 (0.042)
S035	–	20.18	1.55	0.193 (0.005)	-0.252 (0.062)	–	–	0.084 (0.003)	-0.375 (0.054)	–
S037	–	20.08	1.17	0.104 (0.007)	-1.268 (0.086)	0.061 (0.003)	-1.352 (0.050)	–	–	–
S039	–	20.20	1.27	0.087 (0.008)	-1.462 (0.087)	0.040 (0.005)	-1.649 (0.069)	0.033 (0.004)	-1.414 (0.091)	-1.497 (0.047)
S043	–	20.29	1.51	0.179 (0.009)	-0.412 (0.107)	0.155 (0.005)	-0.020 (0.075)	0.058 (0.005)	-0.905 (0.092)	-0.470 (0.053)
S044	–	20.13	1.23	0.068 (0.008)	-1.679 (0.095)	0.016 (0.005)	-1.989 (0.069)	0.046 (0.004)	-1.149 (0.078)	-1.597 (0.046)
S050	–	20.32	1.39	0.161 (0.007)	-0.617 (0.086)	0.078 (0.005)	-1.111 (0.075)	–	–	–
S051	–	20.33	1.28	-0.008 (0.009)	-2.546 (0.099)	–	–	0.053 (0.004)	-1.007 (0.078)	–
S057	–	20.47	1.60	0.198 (0.008)	-0.195 (0.089)	–	–	0.063 (0.004)	-0.803 (0.082)	–
S062	–	20.47	1.61	0.189 (0.008)	-0.298 (0.096)	0.169 (0.004)	0.179 (0.065)	0.064 (0.004)	-0.783 (0.080)	-0.330 (0.046)
S065	–	20.48	1.46	0.136 (0.008)	-0.903 (0.094)	0.141 (0.004)	-0.218 (0.064)	0.063 (0.004)	-0.803 (0.079)	-0.685 (0.046)
S066	–	20.55	1.50	0.178 (0.007)	-0.423 (0.079)	0.160 (0.004)	0.051 (0.055)	0.064 (0.003)	-0.783 (0.067)	-0.413 (0.039)
S070	–	20.43	1.11	0.059 (0.007)	-1.782 (0.079)	0.019 (0.004)	-1.947 (0.058)	0.022 (0.003)	-1.638 (0.069)	-1.780 (0.040)
S072	–	20.52	1.21	0.154 (0.008)	-0.697 (0.099)	0.057 (0.004)	-1.408 (0.070)	0.054 (0.004)	-0.986 (0.082)	-1.001 (0.047)
S075	–	20.63	1.54	0.191 (0.007)	-0.275 (0.077)	0.161 (0.004)	0.066 (0.054)	0.046 (0.003)	-1.149 (0.068)	-0.480 (0.038)
S076	–	20.68	1.19	0.127 (0.009)	-1.005 (0.098)	0.045 (0.005)	-1.578 (0.076)	0.019 (0.004)	-1.699 (0.086)	-1.402 (0.050)
S080	–	20.66	1.32	0.196 (0.009)	-0.218 (0.101)	0.078 (0.005)	-1.111 (0.077)	0.025 (0.007)	-1.577 (0.146)	-1.043 (0.060)
S085	–	20.80	1.42	0.201 (0.006)	-0.161 (0.076)	0.144 (0.004)	-0.175 (0.062)	0.055 (0.004)	-0.966 (0.076)	-0.449 (0.041)
S095	–	20.77	1.23	0.059 (0.010)	-1.782 (0.119)	0.013 (0.006)	-2.032 (0.091)	0.061 (0.005)	-0.844 (0.104)	-1.544 (0.060)
S097	–	20.85	1.31	0.136 (0.007)	-0.903 (0.084)	0.106 (0.005)	-0.714 (0.070)	0.080 (0.004)	-0.457 (0.079)	-0.694 (0.045)
S102	–	20.84	1.19	0.062 (0.008)	-1.747 (0.090)	0.088 (0.007)	-0.969 (0.096)	0.046 (0.003)	-1.149 (0.069)	-1.292 (0.049)
S106	–	20.90	1.30	0.241 (0.008)	0.296 (0.092)	0.085 (0.006)	-1.011 (0.081)	0.055 (0.005)	-0.966 (0.097)	-0.549 (0.052)
S111	–	20.94	1.59	0.197 (0.008)	-0.206 (0.092)	0.192 (0.004)	0.505 (0.059)	0.066 (0.004)	-0.742 (0.082)	-0.211 (0.045)
S113	–	20.99	1.47	0.091 (0.014)	-1.416 (0.156)	0.126 (0.007)	-0.431 (0.095)	-0.013 (0.007)	-2.351 (0.138)	-1.507 (0.076)
S125	–	20.95	1.47	0.169 (0.007)	-0.526 (0.076)	0.125 (0.004)	-0.445 (0.054)	–	–	–
S128	–	21.08	1.59	0.136 (0.009)	-0.903 (0.104)	0.170 (0.006)	0.193 (0.090)	0.067 (0.006)	-0.721 (0.119)	-0.518 (0.060)
S133	–	21.10	1.29	0.066 (–)	-1.702 (–)	0.021 (0.007)	-1.918 (0.100)	-0.010 (0.006)	-2.290 (0.115)	-1.703 (–)
S145	–	21.20	1.48	0.217 (0.009)	0.022 (0.099)	0.114 (0.006)	-0.600 (0.088)	0.038 (0.005)	-1.312 (0.104)	-0.643 (0.056)
S146	–	21.15	1.27	-0.036 (0.012)	-2.866 (0.134)	0.035 (0.008)	-1.720 (0.109)	–	–	–
S151	–	21.21	1.39	0.409 (0.008)	2.214 (0.091)	0.056 (0.008)	-1.422 (0.113)	0.052 (0.009)	-1.027 (0.192)	-0.395 (0.080)
S152	–	21.23	1.23	0.073 (0.012)	-1.622 (0.135)	0.131 (0.006)	-0.360 (0.086)	0.091 (0.005)	-0.233 (0.104)	-0.844 (0.063)
S161	–	21.25	1.16	0.128 (0.009)	-0.994 (0.102)	0.113 (0.006)	-0.615 (0.084)	–	–	–
S162	–	21.36	1.19	0.146 (0.009)	-0.788 (0.105)	0.089 (0.007)	-0.955 (0.099)	0.029 (0.007)	-1.495 (0.136)	-1.119 (0.066)
S163	–	21.33	1.52	-0.042 (–)	-2.934 (–)	0.140 (0.006)	-0.232 (0.092)	0.052 (0.007)	-1.027 (0.141)	-2.929 (–)
S182	–	21.47	1.59	0.335 (–)	1.369 (–)	–	–	0.067 (0.008)	-0.721 (0.165)	–
S185	–	21.46	1.46	0.273 (0.007)	0.661 (0.080)	–	–	0.056 (0.004)	-0.945 (0.093)	–
S194	–	21.43	1.24	0.208 (0.011)	-0.081 (0.120)	0.071 (0.008)	-1.210 (0.112)	0.000 (0.006)	-2.086 (0.125)	-1.137 (0.068)
S200	–	21.55	1.25	0.213 (0.011)	-0.024 (0.122)	0.052 (0.008)	-1.479 (0.109)	–	–	–
S209	–	21.49	1.44	0.020 (0.014)	-2.227 (0.157)	0.093 (0.009)	-0.898 (0.124)	0.072 (0.007)	-0.620 (0.138)	-1.304 (0.081)
S219	–	21.62	1.22	0.087 (–)	-1.462 (–)	0.013 (0.009)	-2.032 (0.126)	-0.056 (0.008)	-3.227 (0.160)	-1.466 (–)
S220	–	21.57	1.17	0.097 (0.009)	-1.348 (0.109)	0.066 (0.005)	-1.281 (0.078)	–	–	–
S223	–	21.68	1.44	0.352 (0.008)	1.563 (0.089)	–	–	0.033 (0.006)	-1.414 (0.125)	–
S229	–	21.63	1.52	0.041 (–)	-1.987 (–)	0.181 (0.006)	0.349 (0.090)	0.053 (0.007)	-1.007 (0.151)	-1.983 (–)
S232	–	21.68	1.52	0.143 (0.010)	-0.823 (0.113)	–	–	0.076 (0.005)	-0.538 (0.114)	–
S242	–	21.67	1.55	0.194 (0.009)	-0.241 (0.103)	–	–	0.067 (0.005)	-0.721 (0.096)	–
S256	–	21.80	1.47	0.312 (0.013)	1.106 (0.144)	–	–	0.071 (0.006)	-0.640 (0.127)	–
S263	–	21.90	1.61	0.143 (0.008)	-0.823 (0.097)	–	–	0.069 (0.005)	-0.681 (0.097)	–
S272	–	21.88	1.30	0.045 (–)	-1.941 (–)	0.053 (0.009)	-1.465 (0.128)	0.092 (0.006)	-0.212 (0.122)	-1.938 (–)
S273	–	21.87	1.18	0.093 (0.012)	-1.393 (0.134)	0.058 (0.008)	-1.394 (0.117)	–	–	–
S278	–	21.79	1.27	0.224 (0.009)	0.102 (0.108)	0.069 (0.008)	-1.238 (0.113)	0.029 (0.007)	-1.495 (0.145)	-0.944 (0.071)
S280	–	21.91	1.56	0.169 (0.013)	-0.526 (0.149)	0.064 (0.007)	-1.309 (0.102)	0.064 (0.006)	-0.783 (0.118)	-0.825 (0.072)
S311	–	22.07	1.53	0.176 (0.010)	-0.446 (0.115)	–	–	0.079 (0.006)	-0.477 (0.129)	–
S318	–	21.97	1.31	0.092 (0.013)	-1.405 (0.145)	0.189 (0.007)	0.462 (0.106)	0.044 (0.007)	-1.190 (0.148)	-0.829 (0.077)
S335	–	22.09	1.48	-0.486 (–)	-8.003 (–)	0.092 (0.008)	-0.912 (0.120)	0.042 (0.007)	-1.231 (0.149)	–
S358	–	22.15	1.48	0.089 (0.010)	-1.439 (0.122)	–	–	0.098 (0.005)	-0.090 (0.110)	–
S363	–	22.22	1.43	0.287 (0.012)	0.821 (0.141)	–	–	–	–	–
S368	–	22.22	1.19	0.212 (0.010)	-0.035 (0.115)	–	–	–	–	–
S369	–	22.26	1.53	0.389 (–)	1.985 (–)	–	–	–	–	–

Table B1 – *continued* IDs, magnitudes, colours, indices and metallicites for the sample.

ID (1)	Alt ID (2)	V (3)	B-R (4)	CH (5)	[Fe/H]$_{CH}$ (6)	Mgb (7)	[Fe/H]$_{Mgb}$ (8)	Fe5270 (9)	[Fe/H]$_{5270}$ (10)	[Fe/H] (11)
S370	–	22.15	1.16	0.079 (0.012)	-1.553 (0.134)	–	–	-0.038 (0.010)	-2.860 (0.207)	–
S376	–	22.21	1.32	-0.126 (0.013)	-3.893 (0.145)	0.044 (0.008)	-1.592 (0.110)	0.090 (0.006)	-0.253 (0.123)	-2.039 (0.073)
S388	–	22.33	1.15	-0.071 (–)	-3.265 (–)	0.060 (0.010)	-1.366 (0.145)	0.118 (0.008)	0.317 (0.170)	-3.256 (–)
S393	–	22.29	1.26	0.132 (0.006)	-0.948 (0.067)	0.075 (0.004)	-1.153 (0.063)	0.041 (0.004)	-1.251 (0.079)	-1.124 (0.040)
S435	–	22.34	1.14	0.197 (0.009)	-0.206 (0.100)	0.036 (0.008)	-1.706 (0.108)	–	–	–
S438	–	22.46	1.32	0.183 (0.014)	-0.366 (0.163)	0.107 (0.008)	-0.700 (0.120)	0.051 (0.008)	-1.047 (0.154)	-0.697 (0.084)
S490	–	22.63	1.19	-0.038 (0.012)	-2.889 (0.133)	0.097 (0.007)	-0.841 (0.108)	0.067 (0.007)	-0.721 (0.138)	-1.514 (0.073)
S502	–	22.68	1.27	0.557 (0.008)	3.903 (0.089)	0.041 (0.010)	-1.635 (0.148)	–	–	–
S529	–	22.93	1.37	-0.022 (–)	-2.706 (–)	–	–	–	–	–
S605	–	23.31	1.61	0.061 (0.006)	-1.759 (0.067)	0.033 (0.003)	-1.748 (0.044)	0.017 (0.003)	-1.740 (0.055)	-1.750 (0.032)